

SANDIA REPORT

SAND96-2772 • UC-704

Unlimited Release

Printed November 1996

Advanced Materials for Aerospace and Biomedical Applications

New Glasses for Hermetic Titanium Seals

Richard K. Brow, David R. Tallant, Stephen V. Crowder, Sambit K. Saha,
Himanshu Jain, Amy McIntyre, Delbert E. Day

Prepared by

Sandia National Laboratories

Albuquerque, New Mexico 87185 and **Livermore**, California 94550

Sandia is a **multiprogram** laboratory operated **by Sandia**

Corporation, a Lockheed Martin Company, for the United States

Department of Energy under Contract DE-AC04-94AL85000.

Approved for public release; distribution is unlimited.

Sandia National Laboratories

Issued by Sandia National Laboratories, operated for the United States Department of Energy by Sandia Corporation.

NOTICE. This report was prepared as an account of work sponsored by an agency of the United States Government. Neither the United States Government nor any agency thereof, nor any of their employees, nor any of their contractors, subcontractors, or their employees, makes any warranty, express or implied, or assumes any legal liability or responsibility for the accuracy, completeness, or usefulness of any information, apparatus, product, or process disclosed, or represents that its use would not infringe privately owned rights. Reference herein to any specific commercial product, process, or service by trade name, trademark, manufacturer, or otherwise, does not necessarily constitute or imply its endorsement, recommendation, or favoring by the United States Government, any agency thereof, or any of their contractors or subcontractors. The views and opinions expressed herein do not necessarily state or reflect those of the United States Government, any agency thereof, or any of their contractors.

Printed in the United States of America. This report has been reproduced directly from the best available copy.

Available to DOE and DOE contractors from
Office of Scientific and Technical Information
P.O. Box 62
Oak Ridge, TN 37831

Prices available from (615) 576-8401, FTS 626-8401

Available to the public from
National Technical Information Service
U.S. Department of Commerce
5285 port Royal Rd
Springfield, VA 22161

NTIS price codes
Printed copy: A04
Microfiche copy: AO1

Advanced Materials for Aerospace and Biomedical Applications

New Glasses for Hermetic Titanium Seals

Richard K. Brow
Glass and Electronic Ceramics Department

David R. Tallant
Surface/Molecular Spectroscopy Department

Stephen V. Crowder
Statistics & Human Factors Department

Sandia National Laboratories
Albuquerque, NM 87185-1349

Sambit K. Saha and Himanshu Jain
Lehigh University
Bethlehem, PA 18015
Sandia Contract No. AF-0924, **AJ-0985**, and AO-4108

Amy McIntyre and Delbert E. Day
University of Missouri-Rolla
Rolla MO 65401
Sandia Contract No. **AF-0923** and **AJ-0984**

Abstract

Titanium and titanium alloys have an outstanding strength-to-weight ratio and corrosion resistance and so are materials of choice for a variety of aerospace and biomedical applications. Such applications are limited by the lack of a viable hermetic glass sealing technology. Conventional silicate sealing glasses are readily reduced by titanium to form interfacial **silicides** that are incompatible with a robust glass/metal seal. Borate-based glasses undergo a **similar** thermochemistry and are reduced to a titanium **boride**. The kinetics of this reactions, however, are apparently slower and so a deleterious interface does not form. Chemically durable **lanthanoborate** glasses were examined as candidate sealing compositions. The compositions, properties, and structures of several alkaline earth, alumina, and **titania** lanthanoborate glass forming systems were evaluated and this information was used as the basis for a designed experiment to optimize compositions for **Ti-sealing**. A number of viable compositions were identified and sealing procedures established. Finally, glass formation, properties, and structure of **biocompatible** Fe₂₀- and TiO₂-doped calcium phosphate systems were also evaluated.

Acknowledgment

The authors thank D. N. Bencoe and M. Dotson of the Glass & Electronic Ceramics Department for preparing and characterizing the **lanthanoborate** glasses; T. V. Montoya and S. D. Rosopo of the Ceramic & Glass Processing Department for preparing the glasses used in the experimental design; C. C. Phifer of the Glass & Electronic Ceramics Department for characterizing the **titanium lanthanoborate** system and for **helpful** discussions throughout the course of this work; R. L. Simpson of the Surface/Molecular Spectroscopy Department for collecting the **Raman spectra**; R. G. Stone and H. L. McCollister of the Ceramic & Glass Processing Department for performing the **titanium** sealing experiments; Dr. G. L. Turner, Spectral Data Services (**Champaign, IL**) for performing the solid state nuclear magnetic resonance spectroscopic analyses.

Contents

Introduction	1
Glass Properties and Structures	2
Lanthanoborate Glasses	2
Alkaline earth lanthanoborates	4
Aluminum lanthanoborates	16
Titanium lanthanoborates	23
Calcium Phosphate Glasses	24
Iron-modified calcium phosphates	24
Titanium-modified calcium phosphates	27
Titanium Sealing Glass Compositions	32
Mixtures Experimental Design	32
Additional Lanthanoborate Sealing Compositions	37
Titanium Sealing	39
Glass/Titanium Interracial Reactions	40
Ti/Glass Interracial Analyses	41
Ti/Glass Reaction Summary	44
Summary and Conclusions	45
References	46
Appendix A	
Publications, presentations, and patents	51
Figures	
2-1 Alkaline earth lanthanoborate compositions examined	5
2-2 Optical properties of alkaline earth lanthanoborate glasses	8
2-3 ¹¹ B MAS NMR spectra from lanthanoborate glasses	9
2-4a Unpolarized Raman spectra from the Mg-La-metaborate glasses	10
2-4b Unpolarized Raman spectra from the Ca-La-metaborate glasses	10
2-4c Unpolarized Raman spectra from the Ba-La-metaborate glasses	11
2-5 Unpolarized Raman spectra from the three 0.71RB ₂ O ₄ •0.29LaB ₃ O ₆ glasses	13
2-6 Aluminum lanthanoborate glass formation	17
2-7 Optical properties of aluminum lanthanoborate glasses	18
2-8 ¹¹ B MAS NMR spectra from the aluminum lanthanoborate glasses	19
2-9 Fraction of tetrahedral borons determined from the ¹¹ B MAS NMR spectra	19
2-10 ²⁷ Al MAS NMR spectrum collected from the 0.25Al ₂ O ₃ •0.75 LaB ₃ O ₆ glas	20
2-11 Unpolarized Raman spectra from the aluminum lanthanoborate glasses	21
2-12 The dependence of the relative concentration of tetrahedral Al sites, determined from the ²⁷ Al MAS NMR spectra, on the modifying cation potential	23
2-13 Titanium lanthanoborate glass formation	24
2-14 Compositions of calcium iron phosphate glasses	25
2-15 Raman spectra collected from binary Fe ₂ O ₃ •P ₂ O ₅	27
2-16 Calcium titanophosphate glasses examined	30
2-17 ³¹ P MAS NMR spectra from xTiO ₂ (1-x)Ca(PO ₃) ₂ glasses	30
2-18 Raman spectra from xTiO ₂ (1-x)Ca(PO ₃) ₂ glasses	31

3-1 Comparisons of the batched and analyzed compositions of the glasses prepared for the experimental design.....	36
3-2 D-cell configuration used to fabricate titanium seals	40
3-3 Titanium seal made with improved sealing glass	40
4-1 Micrographs of titanium/glass reaction interfaces.....	42
4-2 X-ray diffraction pattern from a Ti/silicate glass diffusion couple	43
4-3 Photoelectron spectra from Ti/glass interfaces	44

Tables

2-1 Composition and properties of ternary alkaline earth lanthanoborate glasses.....	6
2-2 Assignment of the Raman bands from the alkaline earth and aluminum lanthanoborate glasses.....	9
2-3 Composition and properties of ternary aluminum lanthanoborate glasses	17
2-4 Compositions of calcium iron phosphate glasses	26
2-5 Compositions and some properties of the titanium phosphate glasses	29
3-1 Batched compositions and properties of the multicomponent glasses prepared for the experimental design	35
3-2 Sealing glass compositions from the experimental design	37
3-3 Approximate compositional ranges (in mole%) for new glasses for titanium hermetic seals	38
3-4 Compositions (mole%) of representative glasses for titanium sealing applications..	38
3-5 Selected properties of different borate-based titanium sealing glasses	39
4-1 Equilibrium contact angles for binary glasses on titanium	41

Advanced Materials for Aerospace and Biomedical Applications

New Glasses for Hermetic Titanium Seals

L Introduction

Titanium and titanium alloys have good strength-to-weight ratios and outstanding corrosion resistance and so are materials of choice for a variety of component applications. For example, the biocompatibility of titanium makes it an attractive material for the construction of implantable medical devices like pacemakers and defibrillator.

Component applications for titanium have been limited by the lack of a commercially reliable hermetic glass sealing technology. Titanium is a highly reactive metal that readily reduces conventional silicate-based glasses during the high temperature sealing process to form a thick, weakly adherent interracial silicide phase that limits the effective strength of the glass-metal seal [Feipeng et al. 1980; Passerone et al. 1977; Brow and Watkins 1987]. One consequence, for example, is the poor adherence of silicate-based bioactive glasses for prosthetic applications [West et al. 1990].

Borate-based glasses form strong bonds to titanium and titanium alloys; pin-pull experiments [Brow and Watkins 1987] indicate that these seals have up to twice the strength of comparable seals made with silicate glasses. Although similar interracial reduction reactions occur during sealing [Brow and Watkins 1987; Brow et al. 1993], it is suspected that such reactions are kinetically limited so that the resulting thin boride interracial phase does not adversely affect the mechanical properties of the seal. Little is known, however, about the nature of these glass-titanium reactions and how they might contribute to the success or failure of a glass seal.

Alkaline earth aluminoborate glasses have been developed for titanium sealing applications [Brow and Watkins 1987; Brow and Watkins 1992]. These glasses have a range of thermal expansion coefficients, including matches to titanium alloys of interest (about $90\text{-}100 \times 10^{-7}/\text{OC}$), and can be sealed at relatively low temperatures (typically $<750^\circ\text{C}$), thus avoiding an allotropic phase transition at 880°C that degrades the mechanical properties of pure titanium. The primary drawback to the use of these glasses is their relatively poor resistance to attack by aqueous solutions. Typical alkaline earth aluminoborate glasses have dissolution rates over 1000 times faster in 70°C deionized water than silicate sealing glasses. This poor chemical durability precludes the use of aluminoborate glasses in component applications where the glass is exposed to the ambient; viz., in an implanted biomedical component.

It was recently reported that glasses in the $\text{TiO}_2 \cdot \text{La}_2\text{O}_3 \cdot \text{B}_2\text{O}_3$ system exhibit outstanding resistance to attack by aqueous solutions [Adams 1990]. A preliminary examination of

lanthanoborate and titanium lanthanoborate glasses revealed chemically durable compositions with the requisite thermal properties for sealing to titanium [Day 1991], although compositions were not optimized for sealing.

Lanthanoborate glasses were first developed as low dispersion, high refractive index optical materials [Kreidl 1983]. La_2O_3 has a beneficial effect on the water resistance of alkaline earth-borate optical glasses [Izumitani 1986]. More recently, lanthanoborate compositions have been developed for high temperature seals in solid oxide fuel cells [Bloom and Ley 1995]. Little is known about the properties and structures of lanthanoborate glasses.

Calcium phosphate-based materials have been used with titanium, for example as a coating [Hayashi et al. 1989], for biomedical applications. The Ca-phosphate base glass is chemically similar to apatite and so would be biocompatible. It is not known if such glasses could be used for hermetic glass/titanium seals.

There were four general goals identified for this LDRD program:

1. *Characterize the relationships between composition, properties, and structure in candidate glass forming systems.* We prepared samples from the alkaline earth lanthanoborate, the aluminum lanthanoborate and the titanium lanthanoborate systems and characterized their molecular-level structures using a variety of spectroscopic probes. In collaboration with the University of Missouri-Rolla, we also investigated Fe_2O_3 - and TiO_2 -modified calcium phosphate glasses.
2. *Develop glass compositions that can be used to make reliable hermetic seals with titanium.* We performed a statistical mixtures design experiment to evaluate the composition-property relationships in a complex seven-component system and determined specific compositions suitable for titanium hermetic seals.
3. *Characterize the reactions that occur at titanium/glass interfaces to understand how reaction kinetics affect seal quality.* In collaboration with Lehigh University, we have used analytical techniques to characterize the interracial reactions that occur when silicate and borate glasses are sealed to titanium.
4. *Transfer the titanium sealing technology to industry.* We have developed techniques to produce hermetic titanium/glass seals and have used these techniques and our new glasses to build prototype seals for several commercial vendors, including seals for anew pacemaker design and anew satellite connector.

II. Glass Properties and Structures

11-1 Lanthanoborate Glasses

There is limited information available about the properties and molecular-level structures of simple lanthanoborate glasses. In the binary $x\text{La}_2\text{O}_3 \cdot (1-x)\text{B}_2\text{O}_3$ system, glass formation is limited to $0.20 \leq x \leq 0.28$ [Levin et al. 1961]; compositions outside this range are phase separated

when quenched. These glasses are refractory, with glass transition temperatures (T_g) around 680°C , and thermal expansion coefficients around $65 \times 10^{-7}/^\circ\text{C}$, densities of 4.1 g/cm^3 , and refractive indices of about 1.72 [Chakraborty et al. 1984]. Properties are generally insensitive to changes in composition within the glass forming region. These glasses have low viscosities at their melting point and so easily devitrify. In fact, the binary composition (mole%) $25\text{La}_2\text{O}_3 \bullet 75\text{B}_2\text{O}_3$ has been identified as the most fragile glass-forming oxide melt [Angell et al. 1989]. The addition of BaO to this composition reduces the activation energy for viscous flow, consistent with an improvement in the glass-forming tendency [Romanova and Nemilov 1970].

Some studies of the structures of lanthanoborate glasses have been reported. Chakraborty et al. [Chakraborty et al. 1984] used Raman and infrared spectroscopy to study the structures of binary lanthanoborate glasses and note a similarity in the spectra of crystalline and amorphous $25\text{La}_2\text{O}_3 \bullet 75\text{B}_2\text{O}_3$, indicating that the glass structure is based on the mixed trigonal and tetrahedral rings found in the crystal. Nemilov et al [Nemilov and Shmatok 1967; Romanova and Nemilov 1970] suggest that Zn- and Ba-lanthanoborate glass structures are based on B-O-B chains, but offer no spectroscopic evidence.

A variety of properties were characterized. Glass transition temperatures (T_g) and crystallization temperatures (TX) were determined by differential thermal analyses (DTA) using a heat rate of $5^\circ\text{C}/\text{min}$ and are reproducible to $\pm 5^\circ\text{C}$. The thermal expansion coefficients were determined by dilatometry using a heat rate of $5^\circ\text{C}/\text{min}$ and are reproducible to $\pm 4 \times 10^{-7}/^\circ\text{C}$. Densities were measured using the Archimedes method with Freon as the buoyancy medium. The average of three measurements are reported; in general, they are reproducible to $\pm 0.002 \text{ g/cm}^3$. Refractive indices were determined using the Becke line method and are accurate to the intervals between our comparative fluids (± 0.002). Finally, the aqueous durabilities of several glasses were determined by measuring weight losses after two weeks in 70°C deionized water. The reported values are the average of three measurements which were generally reproducible to $\pm 50\%$.

The structures of the lanthanoborate glasses prepared for the present work were characterized by Raman spectroscopy and by solid state nuclear magnetic resonance (MAS NMR) spectroscopy. Raman spectra were collected from polished samples by a triple spectrograph equipped with holographic gratings and a charge-coupled detector. The 457.9 nm line of an argon ion laser provided the excitation. The spectrograph was operated at a resolution of 6 cm^{-1} .

¹¹B magic angle spinning nuclear magnetic resonance (MAS NMR) spectra were collected at 116.57 MHz ($H_0=8.45 \text{ T}$), using 2 μsec pulses, 5 sec recycle times, and 200 scans with spinning speeds of 8-10 kHz. The peaks from trigonal and tetrahedral B-sites overlap, adding some uncertainty to the determination of the respective site distributions. We estimate that the reported site concentrations are accurate to $\pm 10\%$. ²⁷Al MAS NMR spectra were collected at 94.67 MHz ($H_0=8.45 \text{ T}$), with pulse widths of 2.1 μsec and 300 msec recycle time, and 3500 scans with spinning speeds of 8-10 kHz; spectra are reported as ppm chemical shifts from $1M \text{ AlCl}_3$. The ²⁷Al MAS NMR spectra were decomposed into Gaussian curves, the areas of which were used as quantitative site concentrations. These areas are reproducible to $\pm 15\%$. Maxima in peak positions are reported for both of these quadrupolar nuclei, not the respective

isotropic chemical shifts. MAS NMR spectra were collected by Spectral Data Services (Champaign, IL).

11-1.1 Alkaline Earth Lanthanoborate Glasses

Brow et al. [1996a] describes in detail our study of the structure and properties of the MgO-, CaO-, and BaO-lanthanoborate glasses. Much of the information described therein is reproduced below.

Glasses were prepared from mixtures of reagent grade H_3BO_3 , La_2O_3 , and the appropriate alkaline earth carbonate, heated to about $1400^\circ C$ in platinum crucibles in air for about three hours. The 50-gram melts were stirred occasionally, before being quenched on steel plates to samples approximately 5 mm thick, and annealed for 30 minutes between $600^\circ C$ and $700^\circ C$. Chemical analyses of the final glasses by inductively coupled plasma-atomic emission spectrometry (ICP-AES) revealed little change in composition after melting; consequently, the 'as-batched' compositions will be used in this report. 50-500 ppm of Cr^{3+} and several rare earth ions were present as contaminants, most likely from the La_2O_3 raw material. Hydroxyl contents were not analyzed and so their effect on glass formation was not considered.

Figure 2-1 shows the Mg-, Ca-, and Ba-lanthanoborate compositions prepared for this study. Closed circles represent compositions for which clear, x-ray amorphous samples about 5 mm thick could be cast from the melt. Open circles represent compositions from which x-ray amorphous glasses could be quenched between steel plates to a thickness generally <1 mm. The crosses represent compositions which either phase separated or crystallized, usually to form LaB_3 , when quenched. In general, we found that the widest range of homogeneous glass formation occurred in the CaO-system and the smallest range of glass formation occurred in the BaO-system; these latter compositions were most prone to phase separation. (We did not examine compositions from the high- B_2O_3 corner of the diagram; viz., $[B_2O_3] > 85$ mole%, nor did we examine binary ROO B_2O_3 compositions). Binary $x La_2O_3 (1-x) B_2O_3$ glasses could be made, with 0.22-0.27, in agreement with the studies by Levin *et al.* [Levin et al. 1961] and Chakraborty, *et al.* [Chakraborty et al 1984; Chakraborty et al. 1985]. These samples required quenching between steel plates to a thickness of about 2 mm to avoid crystallization.

Glass formation in all three alkaline earth lanthanoborate systems is centered on the tie-line between La-metaborate ($La(B_3O_6)$) and the respective alkaline earth metaborate ($R(B_2O_4)$). Similar, limited glass formation has been reported for the Zn-lanthanoborate system [Nemilov and Shrnatok 1967]. Izumitani [1986] reports a somewhat larger BaO- La_2O_3 - B_2O_3 glass forming region, primarily to higher B_2O_3 contents.

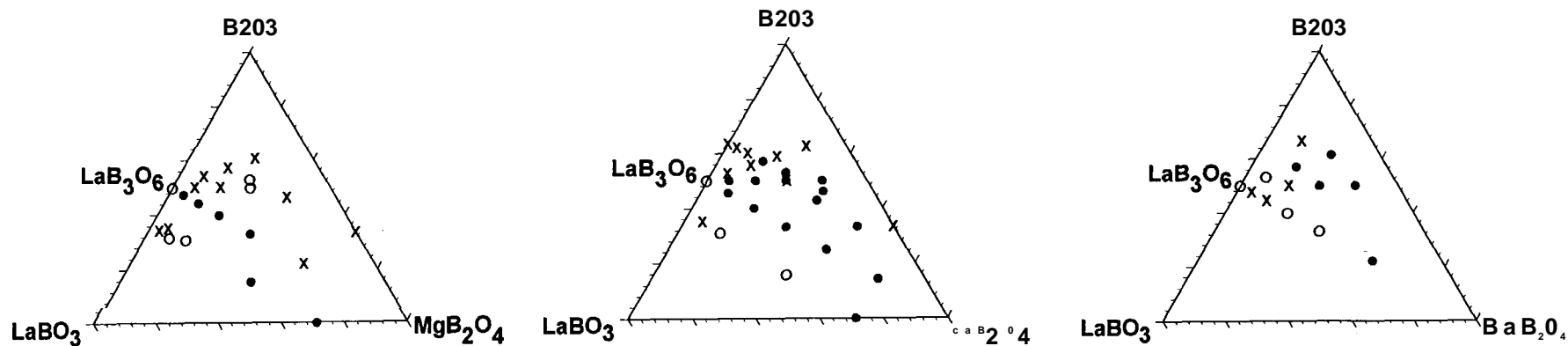


Figure 2-1: Alkaline earth lanthanoborate compositions examined. Closed circles represent compositions which form homogeneous glasses when cast, open circles represent compositions which form homogeneous glasses when quenched between steel plates, and crosses represent compositions which either phase separate or crystallize when quenched.

Table 2-1: Composition and properties of ternary alkaline earth lanthanoborate glasses.

Glass ID	B ₂ O ₃	La ₂ O ₃	CaO	MgO	BaO	CTE (10 ⁻⁶ /°C)	T _g (°C)	T _x (°C)	log DR	density (g/cm ³)	n	MV (cm ³ /mol)	ox. Refr.	Comments
CAML-1	75.00	25.00	0.00	0.00	0.00	65	693	774	-7.3	4.123	1.732	32.42	3.736	qnch. gls.
CAML-2	72.73	22.73	4.55	0.00	0.00	77	669	756	-7.5	4.026	1.727	31.60	3.751	glass
CAML-3	70.00	20.00	10.00	0.00	0.00	81	661	775	-7.5	3.910	1.717	30.56	3.745	glass
CAML-4	66.67	16.67	16.67	0.00	0.00	81	654	781	-7.4	3.795	1.705	29.00	3.699	glass
CAML-5	62.50	12.50	25.00	0.00	0.00	85	648	780	-7.2	3.578	1.692	27.46	3.716	glass
CAML-6	57.14	7.14	35.71	0.00	0.00	90	654	762	-6.6	3.270	1.668	25.41	3.704	glass
CAML-7	72.73	22.73	0.00	4.55	0.00	80	666	757		4.029	1.725	31.40	3.732	glass
CAML-8	70.00	20.00	0.00	10.00	0.00	75	659	769	-7.6	3.897	1.710	30.26	3.711	glass
CAML-9	66.67	16.67	0.00	16.67	0.00	74	657	806	-7.2	3.668	1.688	29.29	3.732	glass
CAML-10	62.50	12.50	0.00	25.00	0.00	76	646	803	-7.1	3.505	1.670	26.91	3.642	glass
CAML-11	57.14	7.14	0.00	35.71	0.00	81	629	763		3.204	1.642	24.17	3.557	part. xtal.
CAML-12	81.82	18.18	0.00	0.00	0.00		679	765		4.026	1.725	28.86	3.393	part. xtal.
CAML-13	80.00	16.67	3.33	0.00	0.00		688	782		3.833	1.705	29.18	3.450	part. xtal.
CAML-14	77.78	14.82	7.41	0.00	0.00		675	790		3.746	1.700	28.45	3.453	part. xtal.
CAML-15	75.00	12.50	12.50	0.00	0.00	70	676	782	-7.2	3.529	1.672	28.32	3.471	glass
CAML-16	71.43	9.52	19.05	0.00	0.00	73	672	823	-7.2	3.253	1.649	28.11	3.551	glass
CAML-17	66.67	5.56	27.78	0.00	0.00	77	661		-6.1	3.026	1.634	26.47	3.552	glass
CAML-18	60.00	0.00	40.00	0.00	0.00		663	757		2.698	1.612	23.79	3.504	qnch. glass
CAML-19	80.00	16.67	0.00	3.33	0.00	79	680	792		3.881	1.712	28.69	3.426	part. xtal.
CAML-20	77.78	14.82	0.00	7.41	0.00	77	675	797		3.728	1.695	28.27	3.437	part. xtal.
CAML-21	75.00	12.50	0.00	12.50	0.00		664	801		3.679	1.698	26.63	3.402	part. xtal.
CAML-22	71.43	9.52	0.00	19.05	0.00	73	660	824		3.527	1.676	25.07	3.325	part. xtal.
CAML-23	66.67	5.56	0.00	27.78	0.00		657	791		3.041	1.636	24.90	3.459	part. xtal.
CAML-24	60.00	0.00	0.00	40.00	0.00		645	733		2.512	1.574	23.05	3.406	crystallized
CAML-25	66.67	27.78	5.56	0.00	0.00			826		4.234		33.08		crystallized
CAML-26	63.64	24.24	12.12	0.00	0.00		669	746		4.219	1.750	30.83	3.876	qnch. glass
CAML-27	60.00	20.00	20.00	0.00	0.00		660	739		4.043	1.735	29.23	3.862	qnch. glass
CAML-28	55.56	14.82	29.63	0.00	0.00		650	742		3.755	1.715	27.58	3.896	qnch. glass
CAML-29	50.00	8.33	41.67	0.00	0.00		634	726		3.400	1.684	25.09	3.857	part. Cryst.
CAML-30	66.67	27.78	0.00	5.56	0.00		669	737		4.310	1.755	32.29	3.895	crystallized
CAML-31	63.64	24.24	0.00	12.12	0.00		665	740		4.167	1.740	30.76	3.869	qnch. glass
CAML-32	60.00	20.00	0.00	20.00	0.00		642	785		4.003	1.725	28.73	3.826	part. xtal.
CAML-33	55.56	14.82	0.00	29.63	0.00	83	650	809		3.760	1.700	26.30	3.757	glass
CAML-34	50.00	8.33	0.00	41.67	0.00	79	647	748		3.335	1.658	23.62	3.692	part. xtal.
CAML-35	72.73	22.73	0.00	0.00	4.55		665	767		4.126	1.727	31.91	3.741	part. xtal.
CAML-36	70.00	20.00	0.00	0.00	10.00	88	656	750		4.145	1.722	31.18	3.737	part. xtal.
CAML-37	66.67	16.67	0.00	0.00	16.67		640	726		4.130	1.713	30.57	3.762	qnch. glass
CAML-38	62.50	12.50	0.00	0.00	25.00	101	620	708		4.126	1.700	29.71	3.773	part. xtal.
CAML-39	57.14	7.14	0.00	0.00	35.71	110	589	696		4.108	1.682	28.68	3.801	glass
CAML-40	62.50	12.50	12.50	12.50	0.00	84	664	831		3.539	1.685	27.21	3.701	glass
CAML-41	62.50	12.50	12.50	0.00	12.50	95	645	742		3.867	1.694	28.55	3.729	glass
CAML-42	62.50	12.50	0.00	12.50	12.50	88	643	762		3.842	1.686	28.23	3.696	glass
CAML-43	50.00	0.00	50.00	0.00	0.00									crystallized
CAML-44	66.67	16.67	0.00	0.00	16.67 (ZnO)	80	620	745						part. xtal.

Table 2-1 summarizes the properties of the alkaline earth **lanthanoborate** glasses. In general, replacing La_2O_3 with an alkaline earth oxide reduces the glass transition temperature and increases the thermal expansion coefficient. Of particular interest for titanium sealing applications are the $\text{BaO-La}_2\text{O}_3\text{-B}_2\text{O}_3$ glasses for which thermal expansions in the range from 90 to $100 \times 10^{-7}/\text{OC}$ are typical. Typical aqueous corrosion rates in 70°C deionized water are about $4 \times 10^{-8} \text{ g/cm}^2 \cdot \text{min}$ for glasses with less than about 20 mole% RO; glasses with higher alkaline earth contents have corrosion rates about 10 times higher. These corrosion rates are at least 100 times lower than those reported for alkaline earth aluminoborate glasses [Watkins et al. 1987; Searstone and Isard 1965], including compositions designed for Ti sealing

Figure 2-2a shows the effect of composition on the molar volume ($V_M = \rho/\text{MW}$, where ρ is the density and MW is the molar weight) of the glasses from the three metaborate systems. In each case, molar volume decreases systematically with increasing substitution by the alkaline earth metaborate, with the **Mg-glasses** possessing the lowest. The implication of these trends is that the addition of the alkaline earth metaborate tightens the structural network of the glass and that **Mg-glasses** have the most dense network and the **Ba-glasses** have the least dense network.

A similar conclusion can be drawn from oxygen refractivity, an optical parameter that is sensitive to changes in glass structure [Kreidl 1989]. The oxygen refractivity, R_{ox} , is the contribution from oxygens to the molar refractivity, R_M , of the glass, calculated from the refractive index and molar volume:

$$R_M = [(n^2 - 1)/(n^2 + 1)] \cdot V_M$$

Both cations and oxygens contribute to the molar refractivity:

$$R_M = \sum N_c R_c + N_{\text{ox}} R_{\text{ox}}$$

where N_c and N_{ox} are the fraction of cations and oxygens, respectively, in the glass, and R_c is the cationic refractivity, assumed to be a constant for each cation and taken from Fanderlik [1 983]. The oxygen refractivity can then be determined after subtracting the cation contributions.

Figure 2-2b shows that the oxygen refractivity of the **Mg-glasses** decreases significantly, the R_{ox} of the **Ca-glasses** decreases slightly, and the R_{ox} of the **Ba-glasses** increases slightly, with the replacement of LaB_3O_6 . This implies that the *average polarizability* of the oxygens in each series increases in the order $\text{Mg} < \text{Ca} < \text{Ba}$. This might result from, for example, a greater fraction of polarizable nonbridging oxygens in the structures of the **Ba-rich** glasses.

Figure 2-3 shows the ^{11}B MAS NMR spectra collected from several different glasses. Each spectrum is dominated by a narrow, symmetric peak centered near +1 ppm due to tetrahedral B-sites [Bunker et al. 1991]. The position of this peak does not change significantly with glass composition. Superimposed on the B(4) peak is a broad, asymmetric feature that extends from about +20 ppm to -12 ppm. This feature is due to **trigonal B-sites**. Second-order **quadrupolar** interactions are responsible for the breadth and asymmetry of this feature [Turner et al. 1986] No attempts were made to determine the quadrupolar coupling constants or asymmetry parameters for these sites.

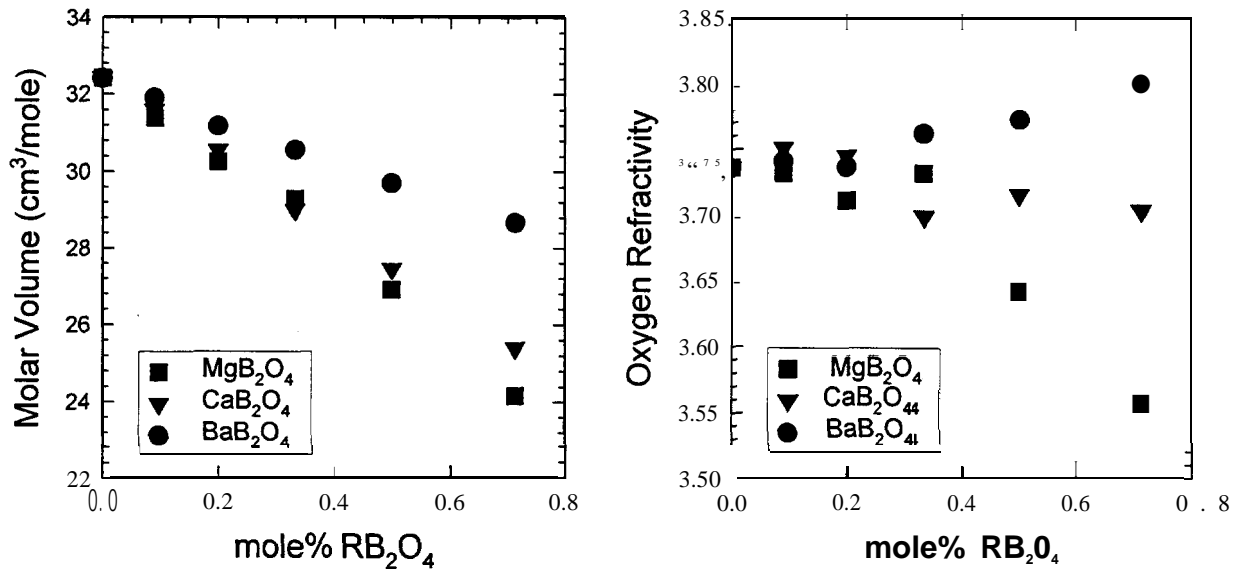


Figure 2-2: Optical properties of alkaline earth lanthanoborate glasses. a) Molar volumes and b) oxygen refractivities for the metaborate compositions.

Figure 2-3 indicates that fewer B(4) species are present in the Mg-glass (0.28), compared to the Ca- and Ba-glasses (0.32 and 0.34, respectively). The binary La-metaborate sample contains the highest fraction of B[4] sites (0.38 ± 0.04 , based on the separate analyses of three different samples).

The Raman spectra from glasses along the respective metaborate tie lines are drawn in Figure 2-4. Spectral interpretation is discussed in detail in [Brow et al. 1996] with reference to assignments summarized in Table 2-2. Trigonal (three-coordinated) boron in the La-metaborate composition is represented by Raman bands apparently peaking near 635 cm⁻¹, but also extending in a broad band to 755 cm⁻¹, (ring and chain metaborates), 840 and 1230 cm⁻¹ (pyroborates) and 930 cm⁻¹ (orthoborates). The Raman band peaking near 1380 cm⁻¹ is associated with the boron-non-bridging-oxygen stretch mode of chain- or ring-type metaborates. Bonding to cations with less propensity for covalent bonding than La³⁺ tends to increase the vibrational frequency of this mode. Tetrahedral borates are represented by Raman bands peaking near 500, 755 and 1090 cm⁻¹. The 500 cm⁻¹ band is generally characteristic of BO₄ tetrahedral. Raman bands peaking in the 750-780 cm⁻¹ region are due to ring structures incorporating BO₄ units, e.g. diborates, triborates, tetraborates, etc. The 1090 cm⁻¹ band appears to be due to diborate units.

As lanthanum is replaced by magnesium, calcium or barium, the Raman band peaking near 1380 cm⁻¹ shifts to higher frequency (see Figures 2-4a-c). As noted above, a higher frequency for these boron-nonbridging oxygen modes is consistent with coordination of chain or ring metaborate structures with cations that bond less covalently than lanthanum.

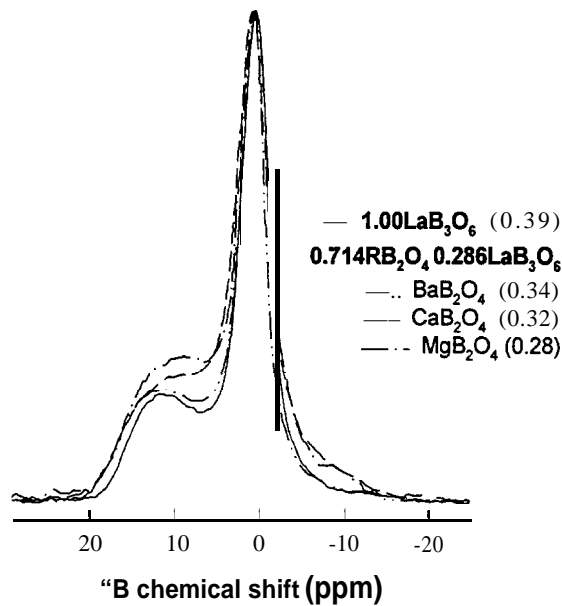


Figure 2.3: ^{11}B MAS NMR spectra from lanthanoborate glasses. The spectra are from the three $0.71 \text{RB}_2\text{O}_4 \cdot 0.29 \text{LaB}_3\text{O}_6$ glasses as well as the LaB_3O_6 glass. The values in parentheses are the relative fractions of tetrahedral-B sites determined by decomposing each ^{11}B NMR spectrum.

Table 2-2: Assignment of the Raman bands from the alkaline earth and aluminum lanthanoborate glasses.

peak position, cm ⁻¹	assignments
450-570	B-O-B stretch, BO_4 units
480-500	Al-O or Al-O-B stretch, aluminate network
600-650	B-O-B stretch, ring metaborates
700-730	B-O-B stretch, chain metaborates
700-720	Al-O or Al-O-B stretch, aluminate network
750-780	B-O-B stretch, rings with BO_4 units; e.g., di-triborates, tri-, tetra-, pentaborates
820-850	B-O-B stretch, pyroborates
890-940	B-O^- stretch, orthoborates
900-1000	B-O-B stretch, BO_4 units; broad, diffuse bands
960-980	Al(4)-O-B(3) stretch, aluminoborate network
1075-1150	B-O- / B-O-B stretch, diborate
1200-1300	B-O^- stretch, pyroborates
1300-1600	B-O stretch, chain and ring metaborates

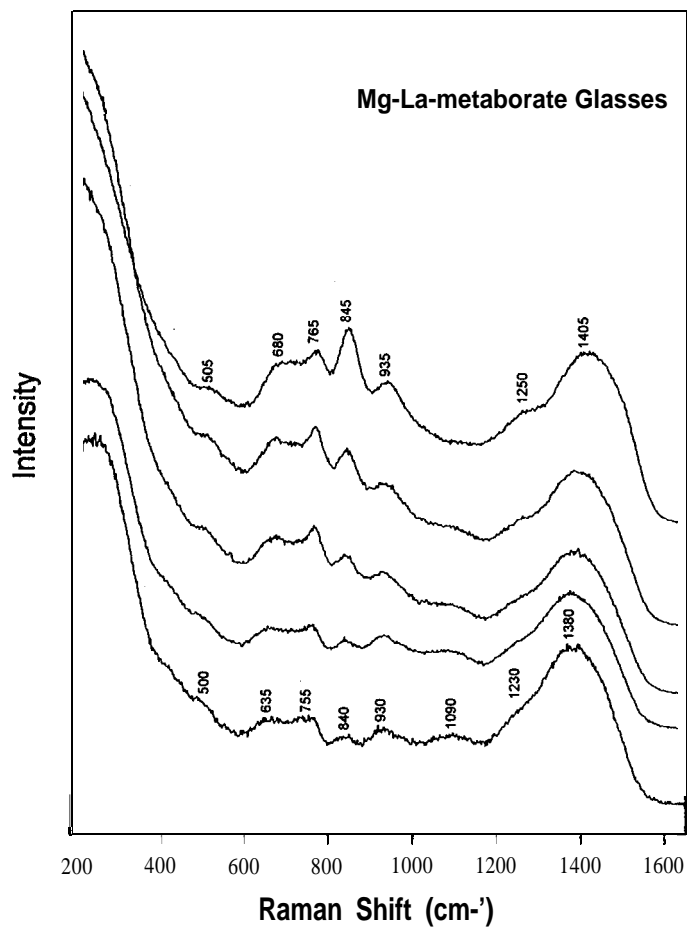


Figure 2.4a: Unpolarized Raman spectra from the Mg-La-metaborate glasses. From bottom to top: 0.00 MgB_2O_4 , 0.09 MgB_2O_4 , 0.33 MgB_2O_4 , 0.50 MgB_2O_4 , and 0.71 MgB_2O_4 .

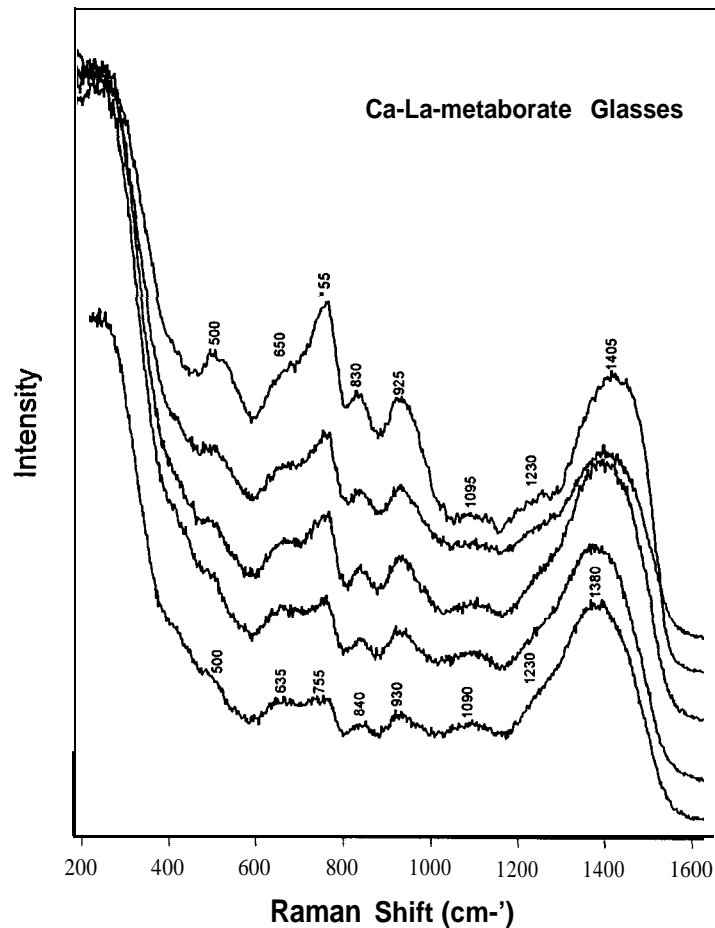


Figure 2.4b: Unpolarized Raman spectra from the Ca-La-metaborate glasses. From bottom to top: 0.00 CaB_2O_4 , 0.09 CaB_2O_4 , 0.33 CaB_2O_4 , 0.50 CaB_2O_4 , and 0.71 CaB_2O_4 .

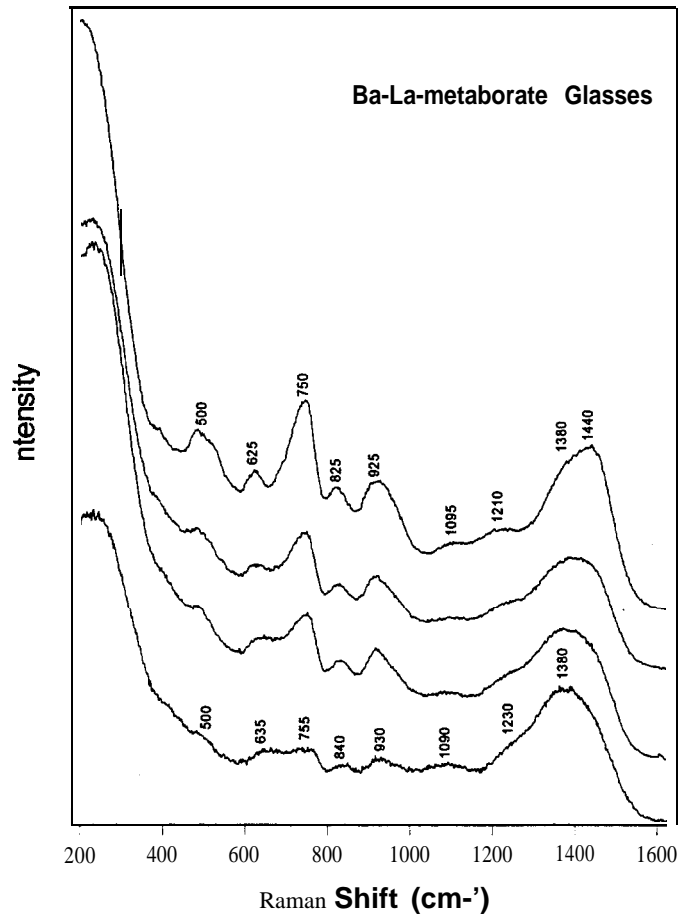


Figure 2.4c: Unpolarized Raman spectra from the Ba-La-metaborate glasses. From bottom to top: 0.00BaB₂O₄, 0.33 BaB₂O₄, 0.50 BaB₂O₄, and 0.71 BaB₂O₄.

With magnesium as the ion substituting for lanthanum (Figure 2.4a), the primary changes in the spectra are an increase in the intensity of the 845 and 1250 cm⁻¹ bands and an increase in frequency of the metaborate band from 635 to 680 cm⁻¹. The increased intensity of the 845 and 1250 cm⁻¹ bands suggests an increase in the number of pyroborate units and, concomitantly, more terminal oxygens. The increase in frequency of the metaborate band may be due to the cation effect (magnesium versus lanthanum) on the vibrational frequencies of metaborate ring structures or it may reflect the development of metaborate chain structures. The envelope of bands near 755 cm⁻¹ in the spectrum of the La-metaborate composition becomes a more distinct peak at slightly higher frequency (765 cm⁻¹) in the spectrum of the composition with the largest magnesium concentration. This more distinct 765 cm⁻¹ band is believed to be due to ring structures with, on the average, fewer BO₄ tetrahedral. The addition of magnesium to the lanthanum borate glass does not appear to increase the concentration of BO₄ tetrahedral in the glass, but it does create more trigonal borate groups with terminal oxygen atoms.

The addition of calcium to the lanthanum borate glass distinctly increases the intensity of bands (500 and 755 cm⁻¹, Figure 2-4b) associated with BO₄ tetrahedral. Metaborate and pyroborate Raman bands do not show a distinct increase in intensity with calcium substitution for lanthanum. There may be some increase in the intensity of the orthoborate band (925 cm⁻¹),

but some of this increase could be due to broad, diffuse Raman bands that occur in the 900-1000 cm^{-1} region and are due to BO_4 tetrahedral.

The relative intensities of the BO_4 -related bands (500 and 750 cm^{-1}) in the spectra from the barium-containing glasses (Figure 2-4c) are greater still than those in the spectra from the calcium-containing glasses. Also, the metaborate band at 625 cm^{-1} , the pyroborate bands at 825 and 1210 cm^{-1} and the orthoborate band at 925 cm^{-1} all become more distinct. The position of the metaborate band at 625 cm^{-1} indicates the retention of ring-type structure in the metaborate groups. The addition of barium causes the largest increase in the intensity of BO_4 -related Raman bands and probably also increases the concentration of terminal oxygens on trigonal borate structures.

The differing effects of the addition of Mg-, Ca-, and Ba-metaborate to the LaB_3O_6 composition are compared in Figure 2-5, in which the Raman spectra from the three $0.29\text{LaB}_3\text{O}_6 \bullet 0.71\text{RB}_2\text{O}_4$ glasses are redrawn. BO_4 -related Raman bands peaking near 500 and 755 cm^{-1} are distinctly more intense in the spectrum of the barium-substituted glass versus the spectrum of the magnesium-substituted glass. The metaborate band (625 cm^{-1}) of the barium-substituted glass is not any more intense than those from the magnesium- and calcium-substituted glasses, but its vibrational frequency is more distinctive of ring metaborate structures. Increased intensity in the spectrum of the barium-substituted glass near 925 cm^{-1} is not necessarily due to more orthoborate groups but may reflect increased intensity in broad, underlying Raman bands due to BO_4 tetrahedral. The relatively high intensity of the Raman band peaking near 845 cm^{-1} in the spectrum of the magnesium-substituted glass indicates an enhanced concentration of pyroborate groups. Barium addition to the lanthanum borate glass enhances the concentration of BO_4 -containing structures relative to magnesium addition, while magnesium addition enhances the concentration of terminal oxygens on trigonal borate groups.

The inset to Figure 2-5 plots the frequency of the lowest frequency peak in the spectra of the three $0.29\text{LaB}_3\text{O}_6 \bullet 0.71\text{RB}_2\text{O}_4$ glasses against the charge-to-radius ratio (ionic potential, z/r) of the metal cations. This band is believed to be due to vibrations of the metal cation with its nearest-neighbor oxygen atoms. The peak frequency of this band increases with the ionic potential of the metal cation, in agreement with trends reported for alkali metaborates [Chryssikos et al. 1994].

Changes in composition have small, yet systematic effects on the properties and structure of the alkaline earth lanthanoborate glasses. In each series, the replacement of $\text{La}(\text{B}_3\text{O}_6)$ by $\text{R}(\text{B}_2\text{O}_4)$ leads to a tighter structural network, as revealed by the systematic decrease in molar volume. The oxygen refractivity data (Fig. 2-2b) suggest that the nature of the oxygen bonding in the three series is different, with the Ba-rich glasses having the greatest average oxygen polarizability. These glasses also have a slightly greater fraction of B(4) sites than their Mg- and Ca-counterparts. In addition, the distributions of anionic borate sites, as indicated by the Raman spectra, depends both on the R:La ratio as well as the type of alkaline earth cation.

These results can be understood if we consider the structures of some of the crystalline end-members of the glass-forming systems. This approach has been used by Chakraborty, *et al.* [Chakraborty et al. 1984; Chakraborty et al. 1985] to understand the vibrational spectra of binary

La-metaborate glasses, and by Chryssikos, *et al.* [1994] to understand effects of structure on glass formation in mixed-alkali metaborates.

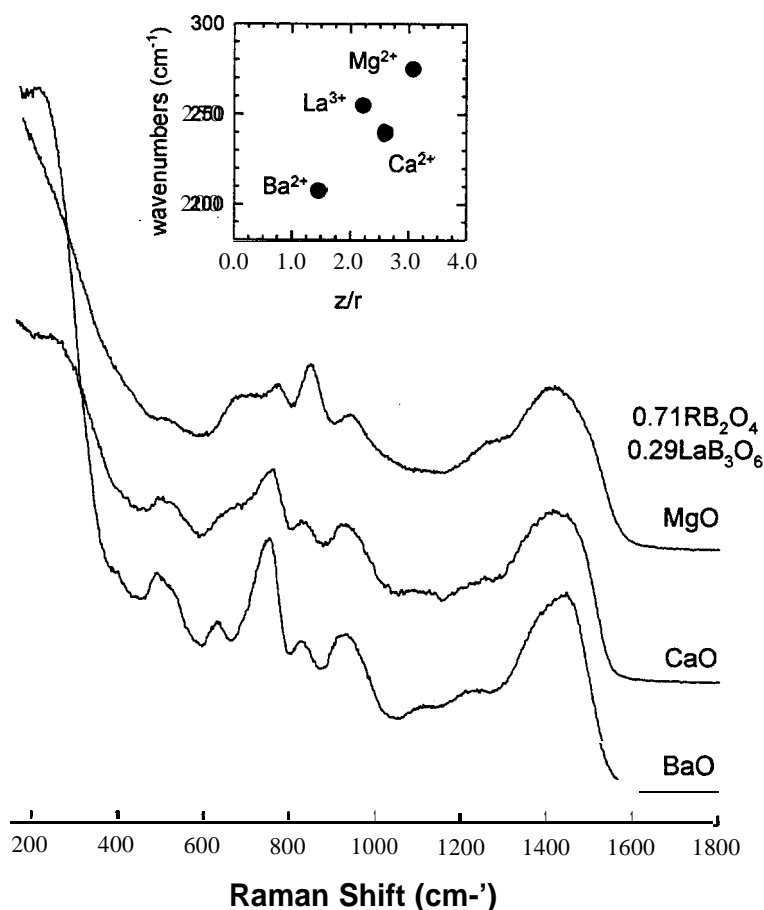
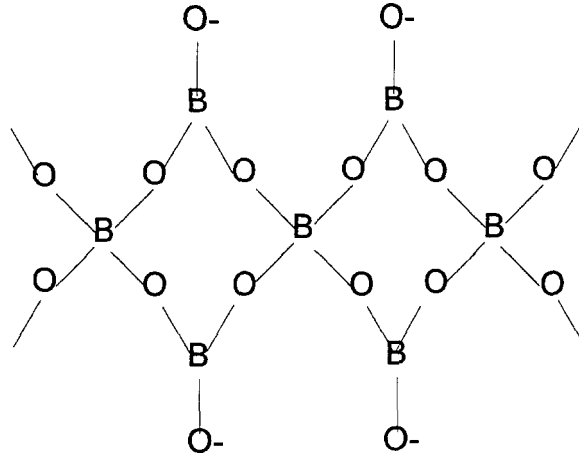


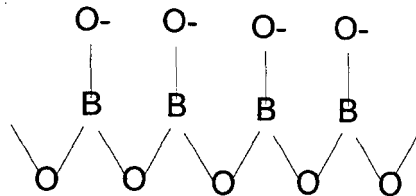
Figure 2-5: Unpolarized Raman spectra from the three 0.71 RB₂O₄•0.29LaB₃O₆ glasses. The inset shows the effect of cationic potential on the frequency of the counterion-oxygen stretching vibrational mode.

Crystalline La(B₃O₆) has a structure based on double chains of **trigonal** (BØ₂O) and **tetrahedral** (BØ₄) species, shown schematically below as metaborate structure I. All four of the oxygens on the B(4) units are shared with neighboring **trigonal** units. Two of the three oxygens on the trigonal unit are bridging and the third is nonbridging. The La ions are found between the chains in ten-coordinated sites to charge-compensate the nonbridging oxygens [St. Ysker and Hoffman 1970].



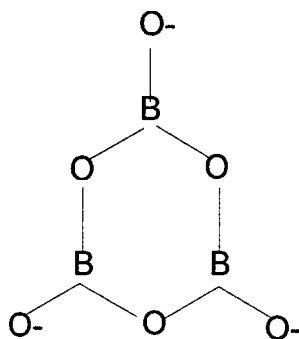
Metaborate Structure I

Crystalline $\text{Ca}(\text{B}_2\text{O}_4)$ has a different borate anionic structure, based on a single chain of **trigonal** borate units [Marezio et al. 1963] shown schematically below as **metaborate structure II**. Each **trigonal** boron ($\text{B}\text{O}_2\text{O}^-$) has one short nonbridging oxygen bond and two longer bridging oxygen bonds. The nonbridging oxygens are charge-compensated by eight-coordinated **Ca**-ions, which then link neighboring **metaborate** chains.



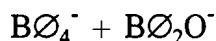
Metaborate Structure II

In contrast to crystalline **Ca**-metaborate, the structure of the low-temperature form of crystalline $\text{Ba}(\text{B}_2\text{O}_4)$ consists of nearly planar B_3O_6 rings [Fröhlich 1984] shown schematically below as **metaborate structure III**. These rings of **trigonal** borons ($\text{B}\text{O}_2\text{O}^-$) are charge-balanced by neighboring eight-coordinated **Ba** ions.



Metaborate Structure III

If a similar structural chemistry controls the anionic species in the alkaline earth lanthanoborate glasses, we would expect that as we replace La^{3+} with R^{2+} , B[4] sites like those in metaborate structure I will be replaced by B [3] sites like those in structures II and III. The ^{11}B MAS NMR spectrum from the binary $25\text{La}_2\text{O}_3 \bullet 75\text{B}_2\text{O}_3$ glass (Fig. 2-3) shows that it does have the highest concentration of B(4) species, approximately 35-40%. The addition of an alkaline earth metaborate (particularly MgB_2O_4) decreases the concentration of tetrahedral sites, consistent with the B(3)-structures (chains and rings) of crystalline $\text{R}(\text{B}_2\text{O}_4)$ compounds:



Raman bands assigned to the metaborate chains (structure II, -720 cm^{-1}) and rings (structure III, -620 cm^{-1}) also increase in relative intensity as R^{2+} replaces La^{3+} , consistent with the replacement of the double-chain, tetragonal-B structure. In addition, the 'ring' peak near 625 cm^{-1} is most distinct in the spectrum from the high-BaO glass (Fig. 2-5), suggesting that the metaborate structure (III) found for $\alpha\text{-BaB}_2\text{O}_4$ is also present in the glass.

The presence of well-defined rings in the Ba/La-metaborate glasses might be related to the smaller range of glass formation if these rings act as nucleation sites in the melt. One suspects that because of steric hindrance, metaborate chains, which appear to be preferred in the Mg- and Ca-glasses, would be less likely to form ordered nuclei as a prelude to crystallization.

The Raman spectra also show that these glasses contain other anionic structures, in addition to the metaborate moieties discussed above. In particular, orthoborate and pyroborate anions are present in glasses with higher RO-contents. Such sites most likely result from the disproportionation of more polymerized borate structures in the respective glass melts; e.g.,



The increase in the relative intensity of the -850 cm^{-1} band in the MgO-glasses suggests a preference for pyroborate species seen in other Raman studies of alkaline earth borate glasses [Kamitsos et al. 1987; Konijnendijk and Stevels 1975].

These **structurally** smaller anionic species most likely contribute to the lower molar volumes in the alkaline earth modified glasses. In particular, the replacement of the large

B(3)/B(4) metaborate double-ring (structure I), preferred by the La-rich glasses, should yield a denser molecular structure as RB_2O_4 is added.

The facile explanation for the trends in the oxygen refractivity data (Fig. 2-2b) is that higher R_{ox} for the Ba-glasses, compared with the Mg-glasses, is due to the presence of a greater concentration of polarizable nonbridging oxygens. It seems plausible that replacing La with an alkaline earth will increase the nonbridging-to-bridging oxygen ratio (compare metaborate structure I with II and III). However, the relative number of nonbridging oxygens seems less sensitive to the type of modifying cation and so the compositional dependence of R_{ox} seems to be instead due to the relative polarizability of those nonbridging oxygens. Duffy and Ingram [1 976] have shown that oxygen refractivity correlates directly with the microscopic optical basicity, a measure of the polarizing tendency of oxygen ions, and that more polarizable oxygens are associated with lower field strength cations. Thus, the trends in the oxygen refractivity data in Fig. 2-2b can be related to the field strengths of the different counterions (inset to Fig. 2-5): replacing La^{3+} with a higher field strength Mg^{2+} ion decreases R_{ox} ; replacing La^{3+} with a lower field strength Ba^{2+} ion increases R_{ox} ; replacing La^{3+} with Ca^{2+} , an ion with a comparable field strength, has little effect on R_{ox} .

11-1.2 Aluminum Lanthanoborate Glasses

The addition of alumina to lanthanoborate glasses reduces the glass transition temperature, increases the thermal expansion coefficient and reduces the molar volume [Chakraborty and Day 1985]. Based on infrared spectra of $0.25\text{La}_2\text{O}_3 \cdot x\text{Al}_2\text{O}_3 \cdot (75-x)\text{B}_2\text{O}_3$ glasses, it was proposed that Al(4) sites substitute for B(4) species in metaborate structure I (section II. 1.1) to form modified $(\text{AlB}_2\text{O}_6)_\infty$ metaborate chains. The relative expansion of the $(\text{AlB}_2\text{O}_6)_\infty$ units, and subsequent weakening of the intra-chain bonds, was used to explain the property variations. However, the polyhedral structures of aluminoborate networks in glasses with high field strength modifying cations (like La^{3+}) are typically much more complex than is suggested by this simple model, since they usually possess Al(5) and Al(6) sites in addition to the tetrahedral aluminums [Bunker et al. 1991].

Figure 2-6 shows the compositions of glasses examined in this study. Closed circles represent compositions that form clear glasses when cast to a thickness of 3-5 mm. Open circles represent compositions which required quenches between steel plates to a thickness < 3 mm to avoid crystallization (determined by x-ray diffraction). Crosses represent compositions which crystallize despite quenching. In general, larger samples of crystal-free glasses could be prepared in the $0.25\text{La}_2\text{O}_3 \cdot y\text{Al}_2\text{O}_3 \cdot (1-y)\text{B}_2\text{O}_3$ series, compared with the $x\text{Al}_2\text{O}_3 \cdot (1-x)\text{LaB}_3\text{O}_6$ series, and glass formation was generally easier for compositions with more than about 15 mole% Al_2O_3 . Glass properties are given in Table 2-3.

Figure 2-7 shows the molar volumes (calculated from glass density and molecular weight, according to $\text{MV}=\text{MW}/\rho$) of the glasses examined in this study along with those reported by Chakraborty and Day [1 985] for the $0.25\text{La}_2\text{O}_3 \cdot y\text{Al}_2\text{O}_3 \cdot (1-y)\text{B}_2\text{O}_3$ series. For both systems, the addition of Al_2O_3 systematically increases molar volume, with no obvious breaks that might indicate a significant change in the structure/composition behavior. Figure 2-7 also shows the refractive indices of glasses in the two series studied here. Again, there are no significant breaks in the compositional dependence of this property.

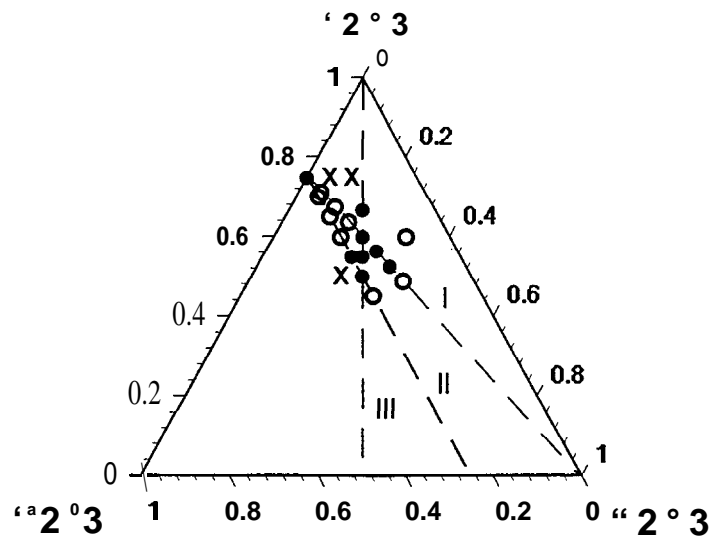


Figure 2.6: Aluminum lanthanoborate glass formation. Line I includes the $x\text{Al}_2\text{O}_3 \cdot (1-x)\text{LaB}_3\text{O}_6$ compositions and line II includes the $0.25\text{La}_2\text{O}_3 \cdot y\text{Al}_2\text{O}_3 \cdot (1-y)\text{B}_2\text{O}_3$ compositions. Open circles represent compositions that readily form glasses and closed circles represent compositions that exhibit minimal crystallization when quenched.

Table 2-3: Composition and properties of ternary aluminum lanthanoborate glasses.

Glass ID	B ₂ O ₃	La ₂ O ₃	Al ₂ O ₃	CTE (10 ⁻⁷ /°C)	T _g (°C)	TX (°C)	density (g/cm ³)	n	ox. Refr.	MV (cm ³ /mol)	Comments
LB-1	75.00	25.00	0.00	65			4.029	1.724	3.799	33.17	qnch. glass
LBA-1	71.25	23.75	5.00	74	666	855	4.027	1.721	3.760	32.79	qnch. glass
LBA-2	63.75	21.25	15.00	68	659	868	3.827	1.700	3.826	33.68	qnch. glass
LBA-3	56.25	18.75	25.00				3.700	1.684	3.836	33.97	glass
LBA-4	70.00	25.00	5.00				4.097	1.730	3.802	33.01	part. xtal.
LBA-5	60.00	25.00	15.00				4.022	1.725	3.958	34.43	part. xtal.
LBA-6A	50.00	25.00	25.00				4.064	1.730	4.031	34.87	qnch. glass
LBA-6	65.00	25.00	10.00	82	637	884	4.088	1.733	3.871	33.48	qnch. glass
LBA-7	55.00	25.00	20.00	81	627	768	4.050	1.725	3.974	34.59	qnch. glass
LBA-8	45.00	25.00	30.00	78	672	797	4.069	1.730	4.074	35.23	qnch. glass
LBA-9	67.50	22.50	10.00	76	659	857	3.938	1.715	3.802	33.13	glass
LBA-10	60.00	20.00	20.00	72	651	866	3.756	1.696	3.859	33.89	glass
LBA-11	52.50	17.50	30.00	67	670	868	3.600	1.679	3.900	34.48	glass
LBA-12	75.00	20.00	5.00	75	655	788	3.855	1.705	3.640	31.76	part. xtal.
LBA-13	75.00	15.00	10.00	69	630	848	3.553	1.682	3.591	31.31	part. xtal.
LBA-14	50.00	30.00	20.00								crystallized
LBA-15	48.75	16.25	35.00		680	904	3.541	1.668	3.878	34.55	part. xtal.
LBA-16	60.00	10.00	30.00	60	688	857	3.131	1.624	3.680	33.50	part. xtal.
LBA-17	66.67	16.67	16.67	64	665	939	3.524	1.660	3.703	33.44	glass
LBA-18	45.00	27.50	27.50	79	678	800	4.201	1.740	4.097	35.45	part. xtal.
LBA-19	70.00	15.00	15.00		645	924	3.503	1.664	3.617	32.22	qnch. glass

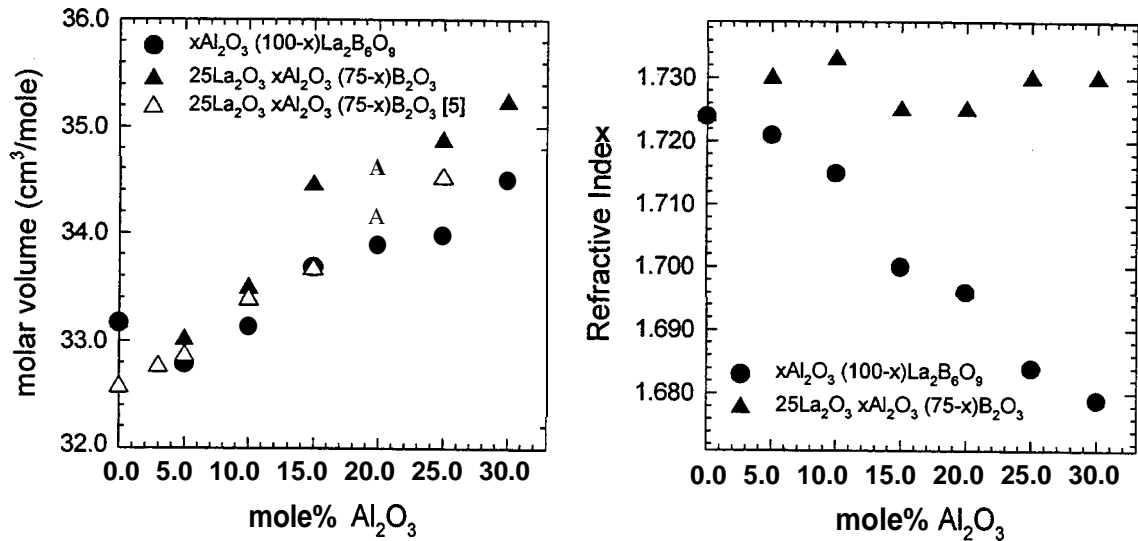


Figure 2.7: Optical properties of aluminum lanthanoborate glasses. (left) The effect of alumina content on the molar volume of $x\text{Al}_2\text{O}_3 \cdot (1-x)\text{LaB}_3\text{O}_6$ glasses (closed circles) and $0.25\text{La}_2\text{O}_3 \cdot y\text{Al}_2\text{O}_3 \cdot (1-y)\text{B}_2\text{O}_3$ glasses examined here (closed triangles) and reported in [Chakraborty and Day 1985] (open triangles); (right) the effect of alumina content on the refractive index of the glasses from the two series prepared in the present study.

Figure 2-8 shows the ^{11}B MAS NMR spectra collected from several of the $x\text{Al}_2\text{O}_3 \cdot (1-x)\text{LaB}_3\text{O}_6$ glasses (Fig. 2-8a) and the $0.25\text{La}_2\text{O}_3 \cdot y\text{Al}_2\text{O}_3 \cdot (1-y)\text{B}_2\text{O}_3$ glasses (Fig. 2-8b). The spectra consist of a relatively narrow, symmetric peak centered at approximately +1 ppm superimposed on a broad, asymmetric feature that extends from about +20 ppm to about -20 ppm. These spectra are qualitatively similar to those reported for alkaline earth lanthanoborate glasses [Brow et al. 1996a]. The narrow peak is due to tetrahedral B-sites [Bunker et al. 1991]. The position of this peak does not change significantly with glass composition. The asymmetric feature is due to trigonal B-sites. Second-order quadrupolar interactions are responsible for the breadth and asymmetry of this feature [Turner et al. 1986].

The relative concentration of tetrahedral B-sites ($N_{\text{B}(4)}$), determined by decomposing each ^{11}B MAS NMR into its two respective contributions, are shown in Fig. 2-9. For both series of glasses, an increase in the alumina content reduces the fraction of tetrahedral boron.

Figure 2-10 shows a representative ^{27}Al MAS NMR spectrum, this collected from the $0.25\text{Al}_2\text{O}_3 \cdot 0.75\text{LaB}_3\text{O}_6$ glass. In general, each spectrum contains three relatively broad, symmetric peaks, centered near +57 ppm, +30 ppm, and +1 ppm. These three broad features are similar to those found in ^{27}Al MAS NMR spectra from alkaline earth aluminoborate glasses [Bunker et al. 1991] and, accordingly, are assigned to $\text{Al}(\text{OB})_4$, $\text{Al}(\text{OB})_5$, and $\text{Al}(\text{OB})_6$ sites, respective y .

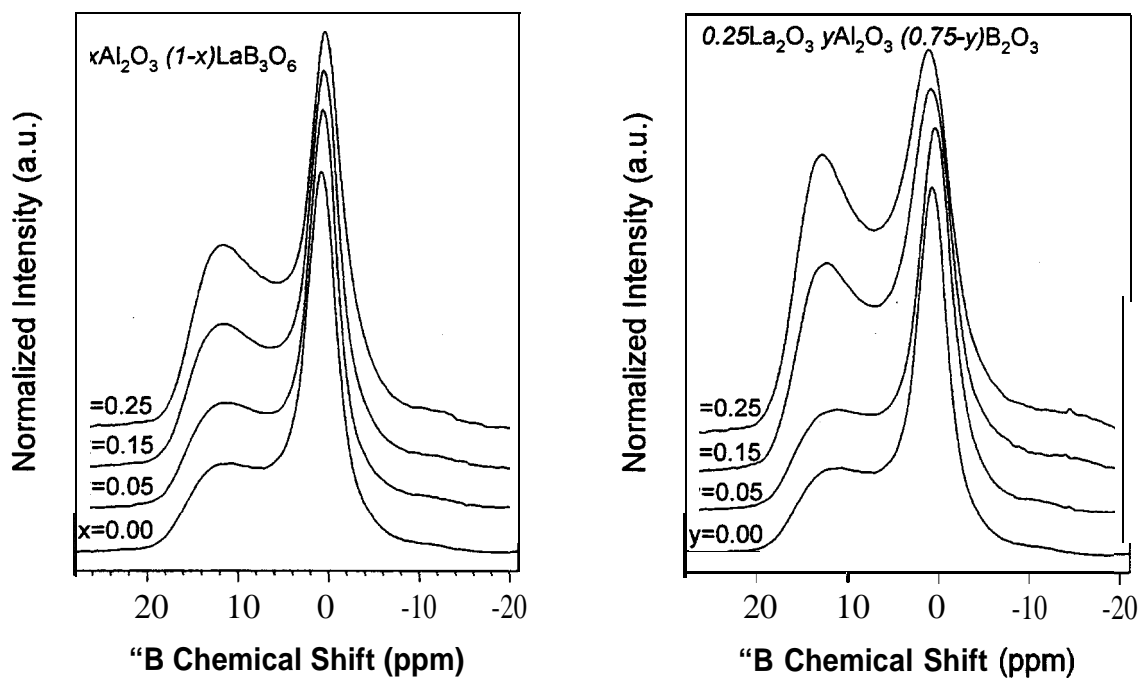


Figure 2-8: ^{11}B MAS NMR spectra from the aluminum lanthanoborate glasses. (left) $x\text{Al}_2\text{O}_3(1-x)\text{LaB}_3\text{O}_6$ series, and the (right) $0.25\text{La}_2\text{O}_3 y\text{Al}_2\text{O}_3(0.75-y)\text{B}_2\text{O}_3$ series.

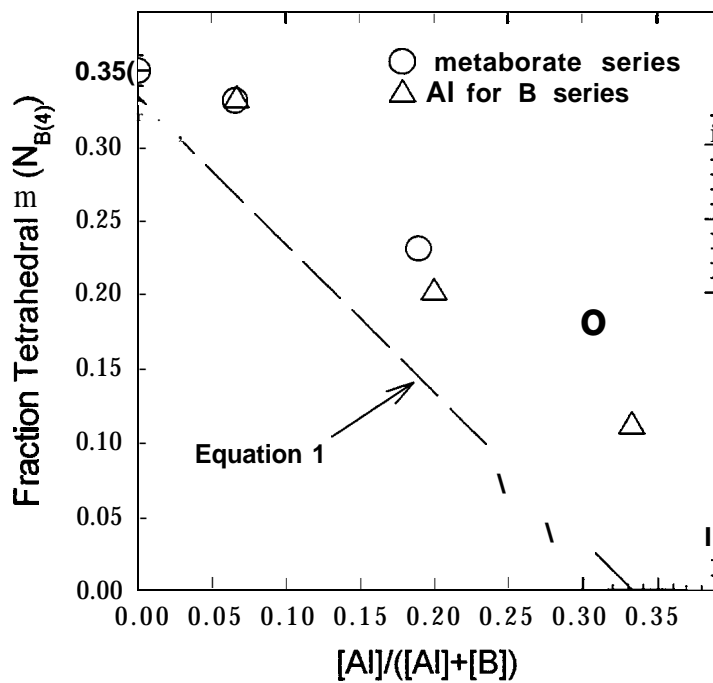


Figure 2.9: Fraction of tetrahedral borons determined from the ^{11}B MAS NMR spectra. The predicted relationship (dashed line) is described in the text,

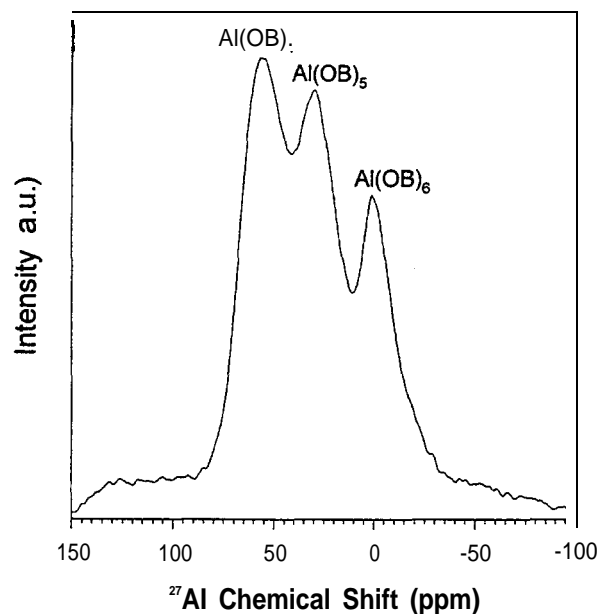


Figure 2-10: ^{27}Al MAS NMR spectrum collected from the $0.25\text{Al}_2\text{O}_3 \cdot 0.75\text{LaB}_3\text{O}_6$ glass.

Figure 2-11 shows the unpolarized Raman spectra collected from several of the $x\text{Al}_2\text{O}_3 \cdot (1-x)\text{LaB}_3\text{O}_6$ glasses (Fig. 2-11 a) and the $0.25\text{La}_2\text{O}_3 \cdot y\text{Al}_2\text{O}_3 \cdot (1-y)\text{B}_2\text{O}_3$ glasses (Fig. 2-11 b). The spectrum from the binary $0.25\text{La}_2\text{O}_3 \cdot 0.75\text{B}_2\text{O}_3$ glass has a series of peaks that can be assigned to a variety of borate structures, including three-coordinated borons in orthoborate units (930 cm^{-1}), pyroborate units (840 and 1235 cm^{-1}), and metaborate ring units (658 and 1380 cm^{-1}). The presence of four-coordinated boron is indicated by Raman bands at $500, 762$ and 1078 cm^{-1} . The last two bands are characteristic of diborate rings which incorporate two B(4) atoms [Konijnendijk and Stevels 1975]. These band assignments are summarized in Table 2-2 above.

In both the metaborate (Fig. 2-11 a) and the Al-for-B series (Fig. 2-11 b), the addition of alumina suppresses or shifts many of the borate peaks shown in the spectrum from the $0.25\text{La}_2\text{O}_3 \cdot 0.75\text{B}_2\text{O}_3$ base glass. In particular, bands associated with tetrahedral borate units in the binary composition are no longer present in the spectra of glasses with 25 mole% Al_2O_3 . New, broad features, at 495 and 711 cm^{-1} , are present in the spectra of glasses with Al_2O_3 -contents over about 15 mole%. These peaks are likely due to aluminate species [McMillan and Piriou 1983]. A highly polarized band near 1000 cm^{-1} is likely due to an aluminoborate network, in agreement with a previous study of a calcium aluminoborate crystal [Fukumi et al. 1984]. New bands at 1205 and 1350 cm^{-1} are B-nonbridging oxygen stretching modes, also presumably associated with an aluminoborate network. Loss of intensity in the Raman band near 658 cm^{-1} , along with the development of intensity near 720 cm^{-1} , indicates the replacement of metaborate rings with chains.

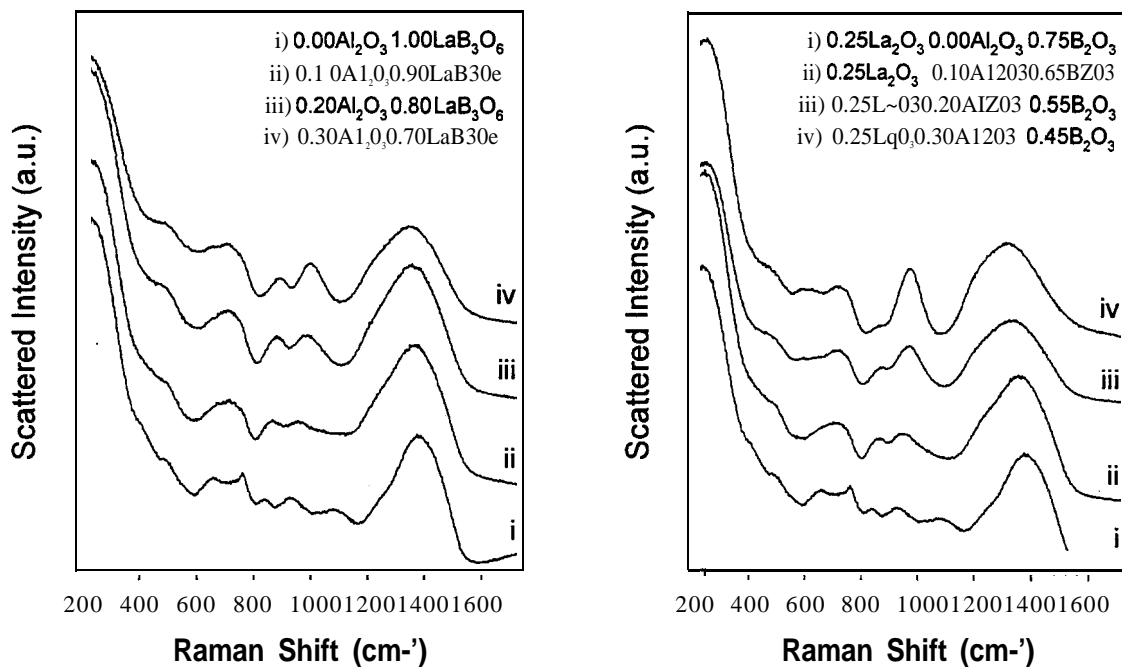
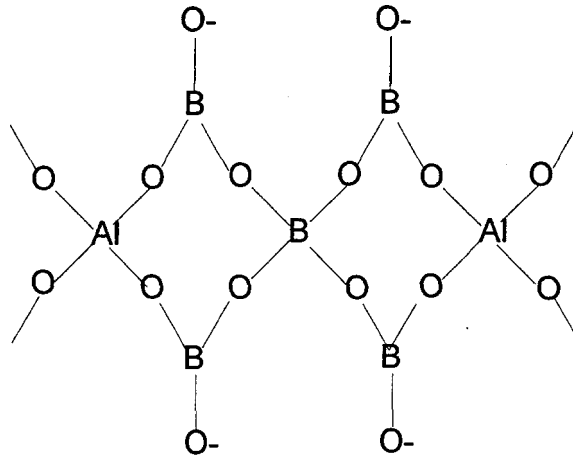


Figure 2-11: Unpolarized Raman spectra from the aluminum lanthanoborate glasses. (left) $x\text{Al}_2\text{O}_3(1-x)\text{LaB}_3\text{O}_6$ series, and (right) $0.25\text{La}_2\text{O}_3 y\text{Al}_2\text{O}_3(1-y)\text{B}_2\text{O}_3$ glasses.

As noted in the previous section, crystalline $\text{La}(\text{B}_3\text{O}_6)$ has a structure based on double chains of trigonal (BO_2O) and tetrahedral (BO_4) species (metaborate structure I), linked by ten-coordinated La^{3+} ions through the nonbridging oxygens. The fraction of borons with tetrahedral coordination in this structure is one-third. According to the ^{11}B MAS NMR results (Figure 2-9), virtually the same fraction (0.38 ± 0.04) exists in the structure of the binary La-metaborate glass. Although the glass structure is somewhat more complex (e.g., the Raman spectrum in Fig. 2-11 reveals the presence of additional borate species, including orthoborate and pyroborate groups), this double-chain metaborate anion seems nevertheless to well-represent the predominant structure in this glass. Evidence for different aspects of this structure in the Raman spectra include the metaborate bands at 658 and 1375 cm^{-1} and the tetrahedral borate ring modes at 762 and 1090 cm^{-1} .

The addition of Al_2O_3 to the lanthanoborate base glass, in both series examined here, increases the molar volume (Fig. 2-7). Chakraborty and Day [1985] proposed that this results from the replacement of smaller B(4) sites in the metaborate anion by larger Al(4) sites (illustrated in the structure below), and indeed, the present spectroscopic results are qualitatively consistent with this general mechanism. The ^{11}B MAS NMR analyses reveal that the fraction of tetrahedral borons decrease. The Raman intensities of tetrahedral boron species also decrease, and the intensities of ‘aluminumoborate’ features (e.g., at 980 cm^{-1}) increase with increasing alumina content.



This model, however, is not quantitatively accurate. If one B(4) site were eliminated by the addition of each Al atom, the fraction of remaining borons that are tetrahedral ($N_{B(4)}$) will be given by:

$$N_{B(4)} = 1/3 - [Al]/([Al]+[B]) \quad (1)$$

Figure 2-9 compares $N_{B(4)}$, determined from the ^{11}B MAS NMR results, with the prediction (dashed line) of equation 1. Clearly, the fraction of tetrahedral borons does not decrease as much as predicted with increasing alumina additions. This is not altogether surprising since the ^{27}Al MAS NMR results show that only about one-third to one-half of the aluminums are present as tetrahedral species; the remaining are incorporated in 5- and 6-coordinated sites (Figure 2-10).

The 5- and 6-coordinated aluminums probably participate in a variety of aluminoborate structures, similar to the aluminoborate linkages thought to co-exist in alkaline earth aluminoborate glasses [Bunker et al. 1991]. These most likely include tri-coordinated oxygens similar to those found in aluminoborate crystals; e.g., oxygens which link 2 tetrahedral borons and one octahedral aluminum, as found in crystalline $CaAlB_3O_7$ [Moore and Araki 1972].

Cations with large electrostatic potentials (defined by z/r , where z is valence and r is ionic radius), like Mg^{2+} , stabilize the formation of more highly charged Al(5) and Al(6) species and La^{3+} appears to have a similar effect. Figure 2.12 shows the effect of modifier potential on the fraction of tetrahedral aluminums found in $25R_xO_y \cdot 25Al_2O_3 \cdot 50B_2O_3$ glasses (the alkaline earth data is from [Bunker et al. 1991]) and La^{3+} is consistent with the previously noted trend. The more highly coordinated aluminums concentrate negative charge on fewer oxygen anions and thus are more readily neutralized by the higher field strength modifiers.

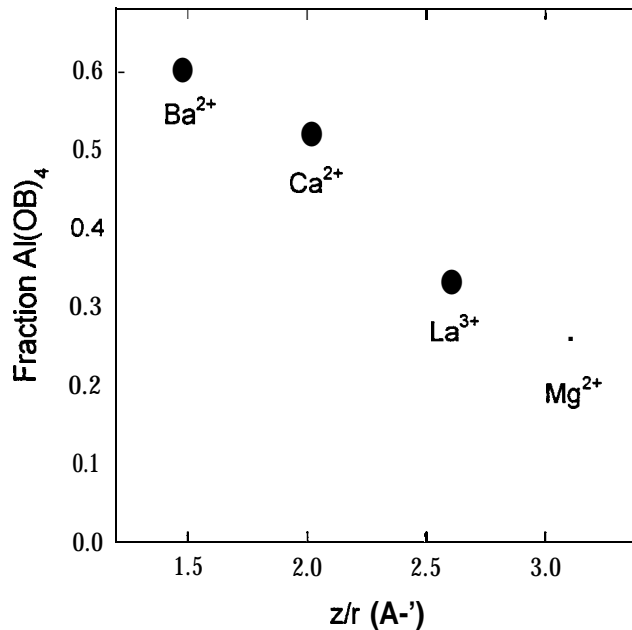


Figure 2.12: The dependence of the relative concentration of tetrahedral Al sites, determined from the ^{27}Al MAS NMR spectra, on the modifying cation potential. The alkaline earth ion results are from ref. [Bunker et al. 1991].

11.1.3 Titanium Lanthanoborate Glasses

Adams [Adams 1990] has reported that glasses prepared from the compositional field bounded by 3-30 wt% TiO_2 , 45-65 wt% La_2O_3 , and 15-45 wt% B_2O_3 have exceptional chemical durabilities, particularly in alkaline solutions.

Phifer [Phifer et al. 1992] prepared and characterized the properties and structures of titanium lanthanoborate glasses. Figure 2.13 shows the region of homogeneous glass formation, centered, more or less, just below the tie-line between lanthanum metaborate ($25\text{La}_2\text{O}_3 \bullet 75\text{B}_2\text{O}_3$) and TiO_2 . Glasses were made in 20 gram batches, melted in platinum crucibles in air between 1200 and 1500°C for about an hour.

In general, expansion coefficient increases (from about 67 to about $75 \times 10^{-7}/^\circ\text{C}$), refractive index increases (from 1.79 to as high as 2.08), and glass transition temperature remains about the same (650-675°C) as the TiO_2 content is increased. The aqueous durabilities of the ternary glasses are excellent. As an example, a glass with the nominal (mole%) composition $25\text{TiO}_2 \bullet 20\text{La}_2\text{O}_3 \bullet 55\text{B}_2\text{O}_3$ dissolved at a rate of $3 \times 10^{-10} \text{ g/cm}^2 \cdot \text{min}$ after 7 days in 70°C deionized water [Day 1991].

Phifer [Phifer unpublished] also performed a variety of spectroscopic studies of the structures of the ternary titanium lanthanoborate glasses. ^{11}B solid state analyses showed little change in the average B-coordination with increasing TiO_2 . Raman analyses indicate that titanium is incorporated primarily as octahedral moieties that cross-link metaborate chains (like those discussed in chapter II-1.1) through the formation of B-O-Ti bonds.

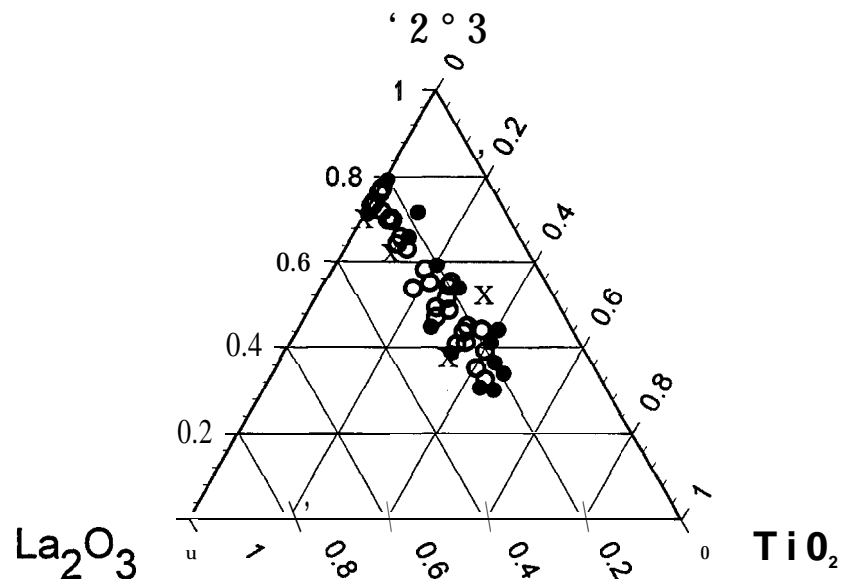


Figure 2.13: Titanium lanthanoborate glass formation. Open circles represent compositions (mole fraction) that readily form glasses, closed circles represent compositions that exhibit minimal crystallization when quenched, and crosses represent compositions which crystallize heavily when quenched (from [Phifer et al 1992]).

It is interesting to note that glass formation in both the titanium and the aluminum lanthanoborate systems extends generally to lower O/13 ratios than was found for the alkaline earth lanthanoborates. This is consistent with the proposed 'glass-forming' roles for both Ti^{4+} and Al^{3+} .

11.2 Calcium Phosphate Glasses

Calcium phosphate based glasses and glass ceramics have been used for a variety of biomedical applications because of their biocompatibility and potential to chemically bond to living bone [Hench 1991; Doremus 1992]. The addition of transition metal oxides (MeO), such as Fe_2O_3 and TiO_2 , to phosphate glass greatly improves its aqueous durability and so the ternary $CaO \cdot MeO \cdot P_2O_5$ systems were investigated for compositions with the requisite thermal and chemical properties for Ti-seals.

11.2.1 Iron-Modified Calcium Phosphate Glasses

The Fe_2O_3 -modified glasses were investigated by the University of Missouri-Rolls (Prof. Delbert E. Day, PI) under contracts AF-0923 and AJ-0984. Details of these studies are contained in two final reports [Day and McIntyre 1994; Day et al 1994]. What follows is a brief summary of those works.

Glasses were prepared from mixtures of $Ca_3P_2O_7$, $NH_4H_2PO_4$, P_2O_5 , and Fe_2O_3 , melted in alumina crucibles at 1100-1200°C for 4 hours in air. The 50 to 80 gram samples were cast in

steel molds and annealed at 500°C for one hour. Figure 2-14 shows the compositions that were prepared; open circles are compositions which form glass, closed circles are compositions which partially crystallized, and crosses are compositions which heavily crystallized. Table 2-4 lists as-batched and analyzed compositions (including some alumina contamination from the crucible, generally less than 1 wt%).

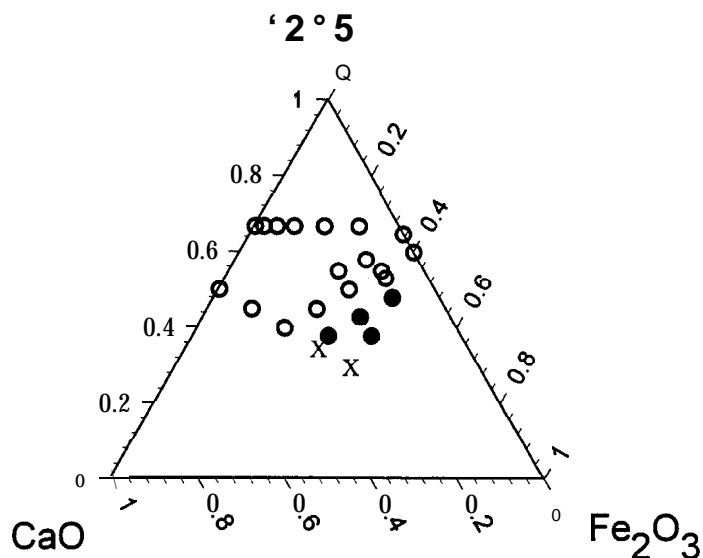


Figure 2-14: Compositions of calcium iron phosphate glasses. Open circles are compositions (mole fraction) which form good glasses, closed circles represent compositions which partially crystallized, and crosses represent compositions which heavily crystallized.

Table 2-4 also lists some of the properties of the glass forming compositions. Thermal expansion coefficient (CTE) was measured by dilatometry from 25 to 300°C at 1°C/min and T_d is the dilatometric softening point. Dissolution rates were determined from weight loss measurements after 64 days in 90°C distilled water. In general, density increases with increasing Fe_2O_3 and CaO contents and T_d increases as CaO replaces P_2O_5 . Glasses with relatively low Fe_2O_3 contents (≤ 10 mole%) have expansion coefficients in the range necessary for matched seals to Ti ($90\text{-}100 \times 10^{-7}/^\circ\text{C}$). The addition of Fe_2O_3 significantly decreases the aqueous dissolution rate (DR) to the point where many of these glasses have superior corrosion resistance to soda-lime silica window glass, which corrodes at a rate of $4 \times 10^{-8} \text{ g/cm}^2\text{-min}$ under identical conditions.

Iron is present as both Fe^{2+} and Fe^{3+} , the latter with increasing relative concentration as the composition becomes more basic; *i.e.*, with decreasing P_2O_5 content. Iron valency was determined by both Mössbauer spectrometry [Day and McIntyre 1994] and by x-ray photoelectron spectroscopy [Brow et al. 1994]. Mössbauer spectrometry indicates that octahedral coordination is preferred.

Table 2-4 Composition (mole%) and properties of calcium iron phosphate glasses.

Glass ID	Batched			Analyzed				Density (g/cm ³)	CTE • 5 (x 10 ⁻¹ /°C)	T _g ±5 (°C)	DR (90°C H.O) (g/cm ² -min)	Comments
	CaO	Fe ₂ O ₃	P ₂ O ₅	CaO	Fe ₂ O ₃	P ₂ O ₅	Al ₂ O ₃					
CFP-1	24.3	9.0	66.7	22.9	9.4	67.2	0.5	2.71	90	530	2.1X10 [*]	Glass
CFP-2	17.3	16.0	66.7	16.7	12.8	69.9	0.6	2.77	74	580	nm	Glass
CFP-3	9.3	24.0	66.7	10.0	21.9	66.2	1.9	2.90	75	550	nm	Glass
CFP-4	12.0	30.0	58.0	13.1	26.5	59.7	0.7	3.05	77	525	7.6x10 ⁻⁹	Glass
CFP-5	20.0	25.0	55.0	19.0	22.7	57.6	0.8	3.07	79	555	7.%10 ⁻⁷	Glass
CFP-6	10.0	37.0	53.0	9.7	23.0	66.7	0.7	2.94	72	562	7.6x10 ⁷	Glass
CFP-7	45.0	10.0	45.0	41.9	8.8	48.7	0.6	3.09	100	582	8.0x10 ⁻⁹	Glass
CFP-8	40.0	20.0	40.0	37.6	18.2	48.7	0.6	3.28	90	585	7.1X10 ⁹	Glass
CFP-9	35.0	30.0	35.0	nm	nm	nm	nm	nm	nm	nm	nm	Xtal
CFP-10	30.0	40.0	30.0	nm	nm	nm	nm	nm	nm	nm	nm	Xtal
CFP-11	20.0	40.0	40.0	nm	nm	nm	nm	nm	nm	nm	nm	Part. Xtal
CFP-12	10.0	40.0	50.0	nm	nm	nm	nm	nm	nm	nm	nm	Part. Xtal
CFP-13	31.3	2.0	66.7	35.8	2.3	61.5	0.4	2.67	100	520	3.0x10 ⁻⁶	Glass
CFP-14	28.3	5.0	66.7	30.2	5.0	64.3	0.6	2.95	95	540	2.5x10 ⁻⁷	Glass
CFP-15	30.0	30.0	40.0	nm	nm	nm	nm	nm	nm	nm	nm	Part. Xtal
CFP-16	20.0	30.0	50.0	16.9	26.8	55.8	0.5	3.20	73	545	1.9X10 ⁻³	Glass
CFP-17	30.0	25.0	45.0	28.5	23.3	47.4	0.5	3.26	90	560	7.1 X10 ⁻²	Glass
CFP-18	20.0	35.0	45.0	nm	nm	nm	nm	nm	nm	nm	nm	Part. Xtal
CFP-19	10.0	35.0	55.0	12.1	29.2	58.7	0.0	3.16	70	517	5.9X10 ⁻¹⁰	Glass
FP-35	0.0	35.3	64.7	9.9	29.5	60.6	nm	2.98	88	495	nm	Glass
FP-40	0.0	40.1	59.9	14.5	31.3	54.3	nm	3.04	77	502	nm	Glass
CP-33	33.3	0.0	66.7	34.2	0.0	64.5	1.3	2.56	100	500	nm	Glass
CP-50	50.0	0.0	50.0	43.8	0.0	51.9	4.3	2.71	100	550	nm	Glass

Raman spectroscopy and photoelectron spectroscopy was used to characterize the structures of binary Fe₂O₃•P₂O₅ and ternary CaO•Fe₂O₃•P₂O₅ glasses. Some representative results are presented below. Details of the XPS analyses of the Fe₂O₃•P₂O₅ glasses can be found in [Brow et al. 1994].

Figure 2.15 shows the Raman spectra collected from several Fe-phosphate glasses prepared at UMR. The spectrum from the glass batched with 15 wt% Fe₂O₃ has peaks that can be attributed to polyphosphate (Q²) chains; i.e., the P-O₂ symmetric (1 187 cm⁻¹) and asymmetric (1261 cm⁻¹) stretching modes and the P-O-P symmetric stretching mode (697 cm⁻¹). The peak at 1062 cm⁻¹ is the P-O₃ stretching mode due to chain terminating (Q¹) sites. With the addition of Fe₂O₃, the bands due to the Q² species are reduced in intensity. The spectra from the 43 and 50 wt% Fe₂O₃ glasses (as batched) are dominated by a single peak centered at 1072 cm⁻¹, again due to the P-O₃ stretching modes of pyrophosphate (Q¹) structures. Of interest is that the Q¹ POP stretching mode, present as a high frequency shoulder to the 697 cm⁻¹ peak in the spectrum from the 15 wt% Fe₂O₃ glass, is either very weak or absent in the spectrum from the 43 wt% Fe₂O₃ glass. Crystalline Fe₂P₂O₇ has pyrophosphate units with a linear P-O-P bond angle [Hoggins et al. 1983]. It is conceivable that similar structures are present in the 43 wt% Fe₂O₃ glass, which has a final composition close to the pyrophosphate [Brow et al. 1994]. The linear P-O-P unit would most likely be Raman inactive, consistent with the weak band shown below.

This evolution of structure, that is the progressive shortening of polyphosphate chains with increasing Fe₂O₃-content by the replacement of P-O-P bonds with P-O-Fe bonds, is supported by our XPS study of similar glasses [Brow et al. 1994]. In that study we showed that

the *O1s* spectra could be decomposed into separate contributions from these two oxygen sites and that their relative intensities were dependent on composition.

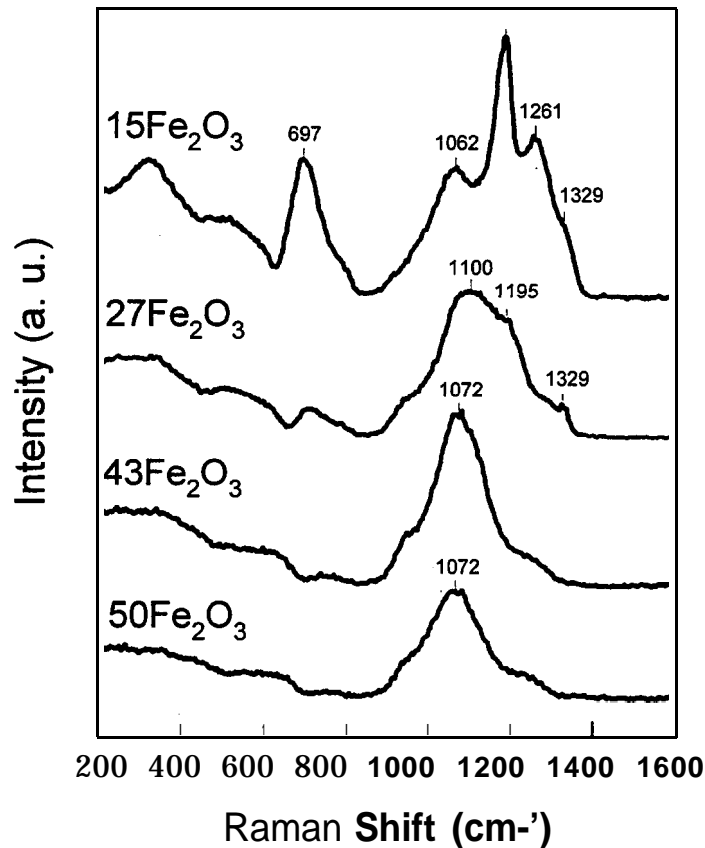


Figure 2-15 Raman spectra collected from binary $\text{Fe}_2\text{O}_3 \cdot \text{P}_2\text{O}_5$. The ‘as batched’ wt% Fe_2O_3 is listed with each spectrum.

Raman spectra were also collected from a number of ternary $\text{CaO} \cdot \text{Fe}_2\text{O}_3 \cdot \text{P}_2\text{O}_5$ glasses. The spectra (not shown) were similar to those collected from the binary $\text{Fe}_2\text{O}_3 \cdot \text{P}_2\text{O}_5$ glasses, indicating that iron has a similar cross-linking effect on structure. This interpretation is consistent with the effect of iron on the properties of Ca-phosphate glasses (Table 2-4). The decrease in CTE and increase in T_d reflects a strengthening of the network as Fe^{3+} replaces either P^{5+} or Ca^{2+} and the general improvement in glass durability most likely results from a decrease in the average phosphate chain length and increase in the number of chemically more stable cross-links with increasing iron content.

II-2.2 Titanium-Modified Calcium Phosphate Glasses

The following is a summary of a paper submitted to *Physics and Chemistry of Glass* on the properties and structure of the calcium titanophosphate glasses prepared for this work [Brow et al. 1996b].

Binary titanophosphate glasses were prepared from mixtures of H_3PO_4 and TiO_2 , melted in alumina crucibles in air for one hour at 1500°C . 10 gram melts were quenched between copper blocks, then checked for crystallinity by x-ray diffraction. Ternary calcium

titanophosphate glasses were prepared from mixtures of CaHP0_4 , $\text{H}_3\text{P0}_4$ and TiO_2 , melted in alumina crucibles in air for up to four hours at 1300-1500°C, depending on the composition. 10-25 gram melts were cast into copper molds, then annealed at about 550°C.

Chemical analyses of representative glasses were done by inductively coupled plasma atomic emission spectrometry (ICP-AES); samples were run in duplicate and the reported results have an uncertainty of $\pm 5\%$ relative. Glass transition and crystallization temperatures were measured by differential thermal analyses at 20°C/min in argon and are reproducible to $\pm 5^\circ\text{C}$. Chemical durabilities were determined as weight loss rates (normalized to sample surface area) from polished samples after four weeks in 100 ml of an agitated saline solution (pH=7.00), contained in Teflon bottles and held at 37°C. Average weight loss rates from four samples, each with a nominal surface area of 3-5 cm^2 , are reported.

X-ray amorphous titanophosphate glasses could be prepared from starting materials with batched TiO_2 contents between 55 and 70 mole%. Melts with greater TiO_2 -contents crystallized upon quenching to form primarily Ti-pyrophosphate and rutile. Chemical analyses reveal some P_2O_5 volatility from the glass melts (Table 2-5), resulting in actual glass compositions with [P]/[Ti] ratios between 0.75 and 1.30. In addition, the 'binary' glasses contain 3-5 mole% Al_2O_3 as a contaminant from the alumina crucible used in glass preparation. These glasses are dark purple, indicating the presence of Ti^{3+} .

Chemical analyses of the ternary calcium titanophosphate glasses (Table 2-5) reveal, in general, that the nominal Ca:Ti:P ratios were retained after melting; there is also, however, some Al_2O_3 pick-up. Glasses become progressively darker with increasing total TiO_2 contents.

Figure 2-16 shows the 'as-batched' compositions of glasses examined in this study. Open circles represent compositions which could be prepared without evidence for crystallization, closed circles are compositions which exhibited slight surface crystallization, and crosses represent compositions which heavily crystallize, despite quenching between copper plates. The solid lines represent the approximate glass forming region reported by Kishioka [1978]. In general, we find a larger region for glass formation than reported by Kishioka, perhaps due to the presence of 3-5 mole% Al_2O_3 in our samples. We find a similar range for glass formation in the $x\text{TiO}_2(1-x)\text{P}_2\text{O}_5$ system to that reported by Hayashi and Saito [1979].

Glass transition temperatures in the binary titanophosphates decrease from 680°C to 637°C with increasing TiO_2 content, as do crystallization temperatures (T_x) (Table 2-6), consistent with the decreasing liquidus temperature reported for the same compositional range [Mal' shikov and Bondar' 1989]. T_g also increases when TiO_2 is added to calcium metaphosphate glass, from 550°C for the $\text{Ca}(\text{PO}_3)_2$ base glass to 689°C for a glass with the nominal composition (mole%) of 45 TiO_2 :55 $\text{Ca}(\text{PO}_3)_2$. Note that the difference between the transition and crystallization temperatures ($T_x - T_g$) decreases with increasing TiO_2 content.

Finally, the normalized weight loss rates in 37°C saline solutions for a number of the glasses are also listed in Table I. The binary titanophosphate glasses are remarkably stable, exhibiting little corrosion after one month on test. The calcium titanophosphate glasses have poorer durabilities than the binary titanophosphates, corroding with weight loss rates that are 1-2

orders of magnitude greater (Table I). In general, the addition of TiO₂ to calcium metaphosphate glass improves its corrosion resistance.

Table 2-5: Compositions and some properties of the titanium phosphate glasses.

Batched			Analyzed				T _g (°C)	TX (°C)	DR (37°C saline) (g/cm ² rein)
CaO	TiO ₂	P ₂ O ₅	CaO	TiO ₂	P*O ₅	Al ₂ O ₃			
..	55.0	45.0	0.0	57.7	37.4	4.9	680	820	1.5X10 ⁻⁷
--	60.0	40.0	0.0	62.5	33.9	3.6	665	818	nm
--	65.0	35.0	0.0	66.9	30.0	3.1	654	796	2.0 x10 ⁻⁹
--	70.0	30.0	1.4	68.2	25.4	5.0	637	694	9 x10 ⁻¹⁰
50.0	0.0	50.0	48.8	0.0	49.8	1.4	550	703	2.3 x10 ⁻⁷
48.7	2.6	48.7	45.1	3.5	47.6	3.8	572	756	nm
47.4	5.3	47.4	45.6	5.0	46.1	3.3	584	773	4.4 x10 ⁻⁸
45.9	8.1	45.9	44.2	8.5	44.6	2.8	596	779	nm
44.4	11.1	44.4	nm	nm	nm	nm	600	766	2.0 x10 ⁻⁸
42.9	14.3	42.9	40.3	15.3	40.6	3.8	634	786	6.1 x10 ⁻⁹
41.2	17.6	41.2	39.1	17.6	39.0	4.2	650	788	6.0 x10 ⁻⁹
39.4	21.2	39.4	41.1	17.7	38.0	3.2	667	765	nm
37.5	25.0	37.5	ml-l	nm	nm	nm			nm
35.5	29.0	35.5	run	nm	nm	nm	689	746	run
50.0	20.0	30.0	nm	run	nm	nm	674	770	1.6 x10 ⁻⁸
40.0	30.0	30.0	39.1	29.3	28.8	2.8	686	755	1.8 x10 ⁻⁹
20.0	44.0	36.0	run	nm	nm	nm	683	746	nm
30.0	30.0	40.0	nm	nm	nm	nm	683	767	nm
20.0	30.0	50.0	20.7	31.1	42.1	6.1	711	815	2.9 x10 ⁻⁹
30.0	20.0	50.0	nm	nm	nm	nm	662	776	3.8 x10 ⁻⁹
10.0	35.0	55.0	nm	nm	nm	nm	590	---	nm

Spectroscopic studies of the structures of the binary TiO₂•P₂O₅ and ternary CaO•TiO₂•P₂O₅ glasses are reported in Brow et al [1996b]. Some of these spectroscopic results are reproduced below.

Figure 2-17 shows ³¹P MAS NMR spectra collected from glasses in the series xTiO₂(1-x)Ca(PO₃)₂. The decrease in chemical shift, from about -27 ppm for x=0.00 to -14 ppm for x=0.35, indicates that the predominant P-moiety is changing from a metaphosphate chain to pyrophosphate-like units. The chemical shift of the most depolymerized sample studied (50CaO 20TiO₂ 30P₂O₅) was -3.8 ppm, indicating that this structure is based on orthophosphate species (see Brow et al [1996b]).

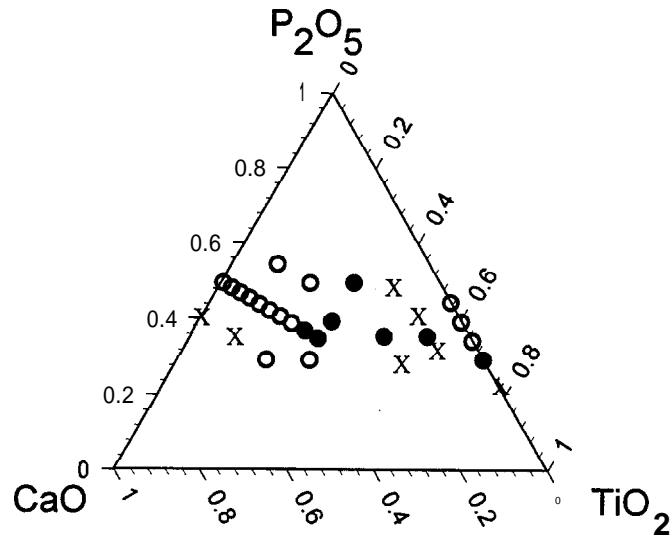


Figure 2-16: Calcium titanophosphate glasses examined. Open circles are compositions which form glass, closed circles are compositions which partially crystallize, and crosses are compositions which heavily crystallize upon quenching.

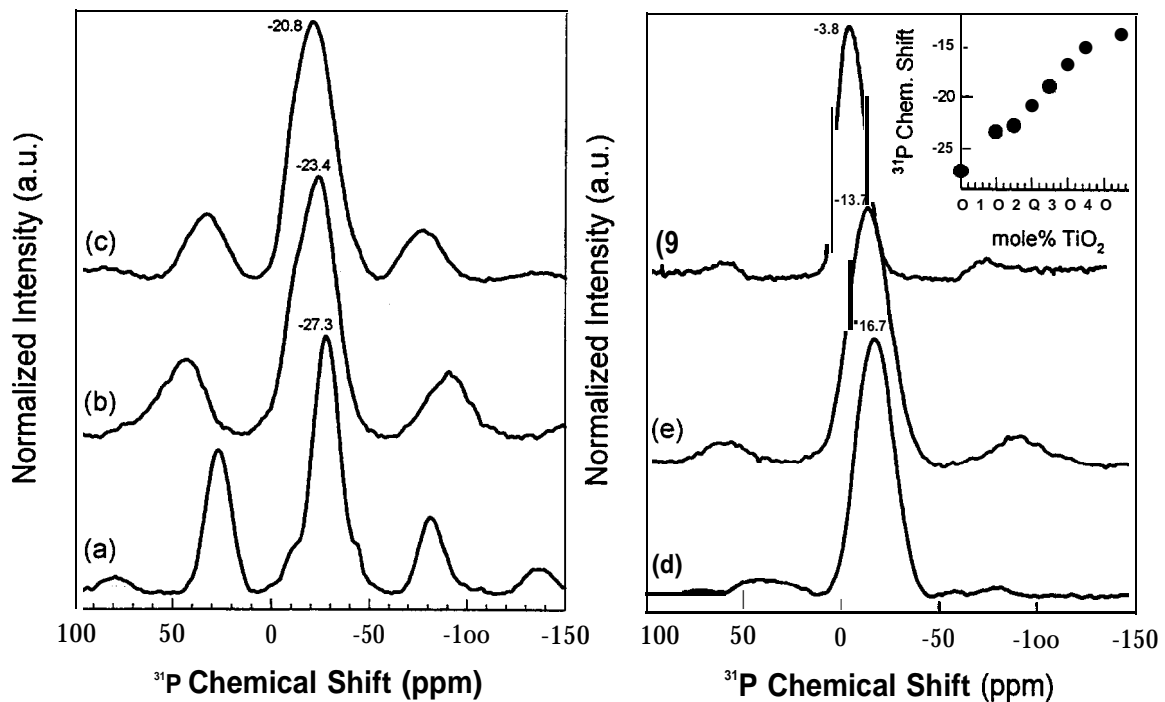


Figure 2.17 ^{31}P MAS NMR spectra from $x\text{TiO}_2(1-x)\text{Ca}(\text{PO}_3)_2$ glasses, where a) $x=0.00$, b) $x=0.10$, c) $x=0.20$, d) $x=0.30$, and e) $x=0.45$. The spectrum from the $50\text{Ca}020\text{Ti}0230\text{P}_2\text{O}_5$ glass is shown in 9. The inset shows the effect of composition on chemical shift for the entire $x\text{TiO}_2(1-x)\text{Ca}(\text{PO}_3)_2$ series.

Figure 2.18 shows Raman spectra collected from glasses in the series $x\text{TiO}_2$ $(1-x)\text{Ca}(\text{PO}_3)_2$. Peak assignments are also discussed in [Brow et al. 1996b]. In general, the decrease in intensity of the band at 1175 cm^{-1} and concomitant increase in intensity of the band at 1020 cm^{-1} reflects the replacement of metaphosphate species with chain terminating pyrophosphate-like units, as supported by the ^{31}P MAS NMR spectra. In addition, new bands at -620 cm^{-1} and 920 cm^{-1} are assigned to the Ti-O stretching modes of titanate structures, including a relatively short titanyl bond in a distorted 5-coordinated structure similar to that reported in other titanophosphate glasses [Cardinal et al. 1995].

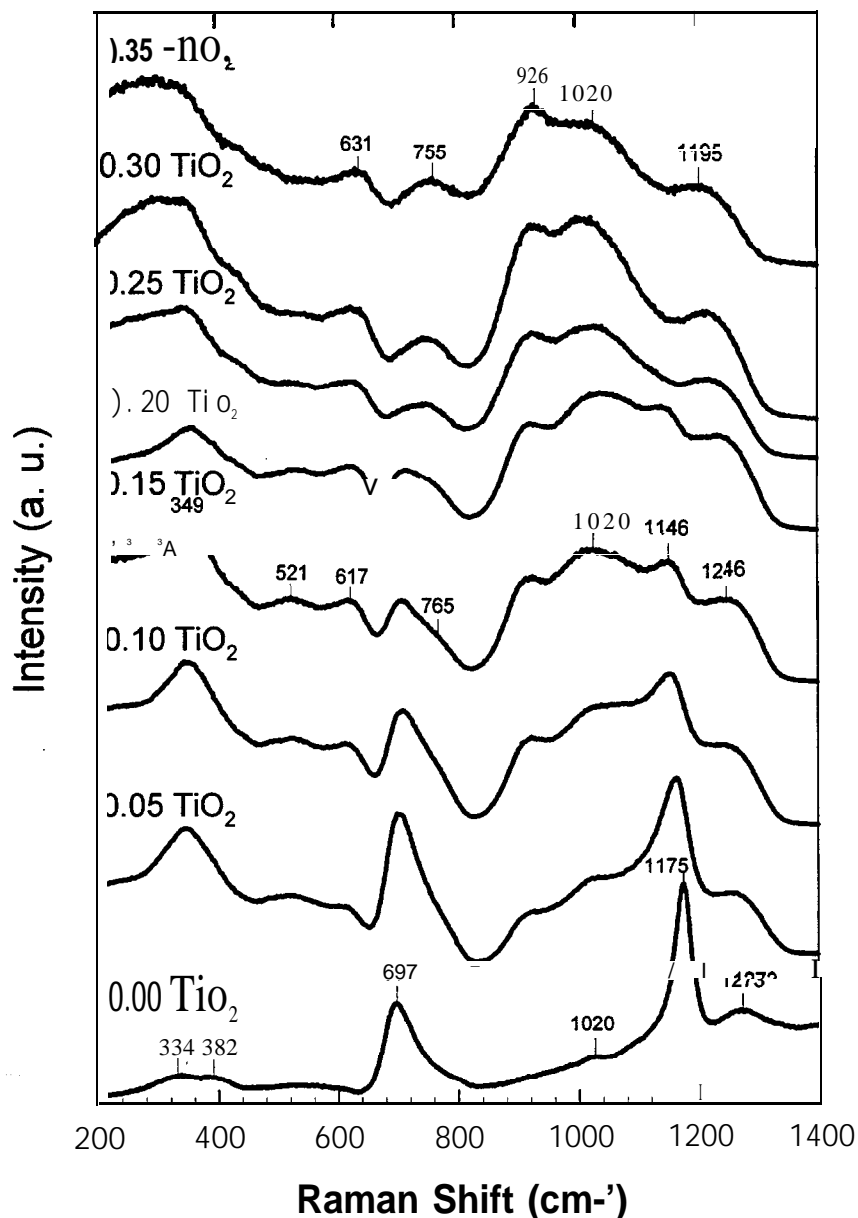
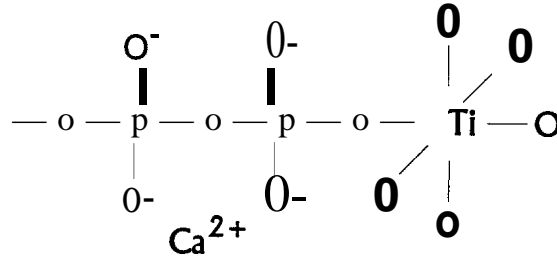


Figure 2.18 Raman spectra from $x\text{TiO}_2(1-x)\text{Ca}(\text{PO}_3)_2$ glasses.

The effect of composition on the $\text{CaO}\cdot\text{TiO}_2\cdot\text{P}_2\text{O}_5$ glass properties can be explained by the cross linking of phosphate chains by titanate polyhedra [Brow et al. 1996b]. One resulting structure is shown in the following schematic, in which an octahedral titanate terminates a phosphate chain. Spectroscopic evidence for the development of such moieties include a

decrease in shielding of the average ^{31}P nucleus with increasing TiO_2 content, indicating a decrease in the average P-chain length, and the development of new bands in the Raman spectra from these glasses, assigned to different Ti-O and Ti-O-P bonds.



Octahedral Fe^{3+} is expected to fill similar structural sites in the calcium iron phosphate glasses discussed in section II-2.1, cross linking increasingly shorter phosphate chains.

III. Titanium Sealing Glass Compositions

III.1 Mixtures Experimental Design

Based on the initial work by Day [1991] and our studies of the alkaline earth, aluminum, and titanium lanthanoborate systems described in sections II. 1.1-3, we selected a five-component system, comprised of B_2O_3 , La_2O_3 , TiO_2 , Al_2O_3 , and CaO , to statistically evaluate for potential titanium sealing compositions. The following mixture constraints (in mole fraction) were initially applied during the calculation of test compositions:

1. $0.30 \leq [\text{La}_2\text{O}_3]/[\text{B}_2\text{O}_3] < 0.625$
2. $0.25 < [\text{TiO}_2]/[\text{B}_2\text{O}_3] \leq 1.30$
3. $0.00 < [\text{Al}_2\text{O}_3]/[\text{B}_2\text{O}_3] \leq 1.00$
4. $0.33 < [\text{CaO}]/[\text{B}_2\text{O}_3] \leq 1.33$
5. $0.00 < ([\text{Al}_2\text{O}_3] + [\text{La}_2\text{O}_3])/[\text{B}_2\text{O}_3] \leq 1.33$
6. $0.40 < [\text{TiO}_2]/[\text{La}_2\text{O}_3] \leq 1.80$
7. $1.00 < [\text{CaO}]/[\text{TiO}_2]$
8. $0.75 < [\text{CaO}]/[\text{Al}_2\text{O}_3] \leq 3.00$
9. $0.325 < [\text{B}_2\text{O}_3] \leq 0.75$

The software program MIXSOFT [Piepel 1992] was used to generate a set of candidate points consisting of the extreme vertices, one-dimensional, two-dimensional, three-dimensional, and overall centroid points.

Number of Extreme Vertices	=23 points
Number of 1-D Centroids	=46 points
Number of 2-D Centroids	=33 points
Number of 3-D Centroids	= 10 points
<u>Overall Centroid</u>	<u>= 1 point</u>
Total Number of Candidates	= 113 points

An additional constraint involving the oxygen-to-boron ratio ($2.0 \leq [\text{O}]/[\text{B}] \leq 3.5$) reduced the number of candidate points to 71 (13 extreme vertices, 28 1-D centroids, 21 2-D centroids, 8 3-D centroids, and 1 overall centroid). The DETMAX (Determinant Maximization) algorithm was used to select a subset consisting of 20-22 design points from the 71 candidate points.

A useful criterion for evaluating a mixtures experimental design is the V-max criterion. If $Y_p(\mathbf{x})$ represents the estimated response at the design point \mathbf{x} , then

$$V\text{-max} = \max \{ \text{Var}(Y_p(\mathbf{x})) \}, \text{ overall } \mathbf{x}=(x_1, x_2, x_3, x_4, x_5)$$

in a set of candidate design points. V-max is thus the maximum value of the estimation variance, $\text{Var}(Y_p(\mathbf{x}))$, over all points in the design space. Snee [1975] comments that any design with V-max < 1.002 indicates a good design from a practical viewpoint, because this implies that the model estimations, $Y_p(\mathbf{x})$, are as precise as the measured responses (σ^2 here is the experimental error variance). The V-max criterion was used to check the designs generated by the DETMAX algorithm to choose a good design for estimating the parameters of a full quadratic model. The initial design for this study has V-max = $0.98\sigma^2$ (with one center point) and V-max = $0.97\sigma^2$ (with three center points). The design with three center points was chosen because replication of the center point provides a 'stability check' throughout the course of the experiment.

A random melt run order was determined for the compositions. Table 3-1 lists the compositions by run ('TIG-1' through 'TIG-23') and by melt number. Each composition was prepared from reagent grade H_3BO_3 , La_2O_3 , TiO_2 , Al_2O_3 , and CaCO_3 . Batches were calculated to prepare 500 gram samples. The batches were generally melted at 1300°C for 4-6 hours (including two hours of stirring) in air in platinum crucibles. Glasses were generally cast into preheated molds, then annealed near the glass transition temperature.

Many of the compositions identified for the experimental design crystallized when cast (see comments in Table 3. 1). In particular, alumina appears to enhance crystallization in some of the compositions and TiO_2 appears to promote glass formation. The compositional constraints listed above were modified accordingly:

1. $0.20 \leq [\text{La}_2\text{O}_3]/[\text{B}_2\text{O}_3] \leq 0.50$
2. unchanged
3. unchanged
4. $0.33 < [\text{CaO}]/[\text{B}_2\text{O}_3] \leq 1.00$
5. unchanged
6. $0.00 < [\text{TiO}_2]/[\text{La}_2\text{O}_3] \leq 2.50$
7. eliminate
8. eliminate
9. $0.30 < [\text{B}_2\text{O}_3] \leq 0.75$

The effective compositional space for this experiment then becomes:

- 32 mole% $< \text{B}_2\text{O}_3 \leq 57$ mole%
- 9 mole% $< \text{La}_2\text{O}_3 \leq 21$ mole%
- 0 mole% $< \text{TiO}_2 \leq 34$ mole%
- 0 mole% $< \text{Al}_2\text{O}_3 \leq 27$ mole%

9 mole% < CaO ≤ 42 mole%

Six additional compositions ('TIG-24' through 'TIG-29') were then identified, using the statistical procedures outlined above, and prepared..

Glass compositions were determined by inductively coupled plasma atomic emission spectrometry (ICP-AES). Glasses were pulverized, dried, then digested in a variety of acids, spiked with an internal standard and then analyzed against certified standard solutions. Samples were prepared in triplicate and analyzed in replicate for statistical purposes. In general, the analyzed and batched compositions were comparable (see Figs 3-1 a-e for comparisons). The analyzed compositions were used in the mixtures experiment calculations.

Three properties were identified as experimental response variables. These were the coefficient of thermal expansion (CTE, measured from 25 to 500°C), The difference (ΔT) between the crystallization temperature (from the onset of the first crystallization peak in the DTA curve) and the glass transition temperature (T_g , calculated from the peak of the first derivative of a differential thermal analysis, DTA, curve), and aqueous durability (DR, measured as a weight loss rate, normalized to sample surface area, after two weeks in deionized water at 70°C). These properties are also given in Table 3-1.

Empirical polynomial models were constructed for the three response variables starting with a linear model such that:

$$\text{Response } Y = \beta_1 X_1 + \beta_2 X_2 + \beta_3 X_3 + \beta_4 X_4 + \beta_5 X_5 + \varepsilon, \quad (\text{III-1})$$

where the β_i s are the coefficients to be estimated and ε represents a random experimental error term with the expected value $E(\varepsilon) = 0$ and variance $\text{Var}(\varepsilon) = \sigma^2$. In addition, many of the important quadratic terms that could be added to model (III-1) were determined from a statistical analysis of the data. The following models that fit the experimental data were generated.

$$\text{CTE} = 0.318(0.066) * \text{B}_2\text{O}_3 + 1.65(0.327) * \text{La}_2\text{O}_3 + 0.865(0.079) * \text{TiO}_2 - [0.396(0.025) * \text{Al}_2\text{O}_3] + 1.70(0.061) * \text{CaO} + [0.0394(0.025) * \text{La}_2\text{O}_3 * \text{Al}_2\text{O}_3]$$

$$\Delta T = 6.97(1.36) * \text{B}_2\text{O}_3 - 23.5(6.36) * \text{La}_2\text{O}_3 - 12.3(5.05) * \text{TiO}_2 + 8.16(1.20) * \text{Al}_2\text{O}_3 - 7.63(2.37) * \text{CaO} + 0.946(0.316) * \text{La}_2\text{O}_3 * \text{TiO}_2 + 0.702(0.273) * \text{La}_2\text{O}_3 * \text{CaO} + [0.202(0.100) * \text{TiO}_2 * \text{CaO}]$$

$$\text{Log(DR)} = -0.022(0.005) * \text{B}_2\text{O}_3 - 0.308(0.018) * \text{La}_2\text{O}_3 - 0.102(0.006) * \text{TiO}_2 - [0.052(0.008) * \text{Al}_2\text{O}_3] - 0.046(0.005) * \text{CaO}$$

Standard errors of the estimates are in parentheses. Terms in brackets [-] are only marginally significant (at 80% confidence level).

Table 3.1 Batched compositions and properties of the multicomponent glasses prepared for the experimental design.

Glass ID, melt #	B ₂ O ₃	La ₂ O ₃	TiO ₂	Al ₂ O ₃	CaO	MgO	BaO	CTE (10 ⁻⁶ /°C)	T _g (DTA) (°C)	T _x (DTA) (°C)	log DR	Comments
TIG-1, A93011	36.00	11.00	0.00	25.00	28.00	0.00	0.00	81	666	843	-7.0	not clear, sit. greenish tint, translucent (phase sep).
TIG-2, A93012	40.00	25.00	0.00	9.00	26.00	0.00	0.00	--	--	--	--	opaque, lt. yellow, little quenched glass
TIG-3, A93013	58.00	17.00	0.00	6.00	19.00	0.00	0.00	83	624	731	-7.6	lt. greenish blue, wht layer surf. xtals on slabs
TIG-4, A93014	48.00	15.00	0.00	21.00	16.00	0.00	0.00	75	654	895	-7.4	sit. bluish tint, glass covered w/ thin skin of surf. xtals.
TIG-5, A93015	38.00	21.00	12.00	17.00	12.00	0.00	0.00	83	683	793	<-10	greenish tint, layer of wht. surf. xtals, some bulk xtals.
TIG-6, A93017	38.00	16.00	29.00	4.00	13.00	0.00	0.00	89	663	793	<-10	goldish tan, surf. xtals on slabs, other parts clear
TIG-7, A93018	33.00	10.00	0.00	14.00	43.00	0.00	0.00	99	639	742	-6.7	green yellow, one slab extensive surf. xtals., other slab clear
TIG-8, A93019	41.00	25.00	16.00	5.00	13.00	0.00	0.00	--	--	--	--	opaque, heavily xtallized
TIG-9, A93020	38.00	11.00	21.00	17.00	13.00	0.00	0.00	74	659	823	-8.0	excellent glass, goldish tan, mostly clear, some surf. xtals.
TIG-10, A93022	53.00	16.00	0.00	14.00	17.00	0.00	0.00	76	653	780	-7.7	greenish blue tint, thin skin of surf. xtals. over glass
TIG-11, A93023	44.00	13.00	24.00	5.00	14.00	0.00	0.00	77	660	797	-8.6	goldish tan, wht. surf. xtals around slab edges
TIG-12, A93025	40.00	12.00	0.00	28.00	20.00	0.00	0.00	71	658	859	-7.3	greenish blue, no surf. xtals, glass has clear dendritic xtals.
TIG-12, A93038	40.00	12.00	0.00	28.00	20.00	0.00	0.00	73				
TIG-13, A93026	32.00	15.00	0.00	13.00	40.00	0.00	0.00	--	--	--	--	opaque, brown, thin glass layer on quenched surfaces
TIG-14, A93027	37.00	15.00	11.00	14.00	23.00	0.00	0.00	88	650	811	-8.5	green tint, glass has thin skin of surf. xtals, some clear pieces
TIG-15, A93028	32.00	10.00	0.00	19.00	39.00	0.00	0.00	91	647	764	-6.6	yellowish green, layer of white surf. xtals. on slabs
TIG-16, A93029	37.00	15.00	11.00	14.00	23.00	0.00	0.00	90	649	811	-8.4	greenish layer of white surface xtals. on slabs
TIG-17, A93030	51.00	15.00	12.00	5.00	17.00	0.00	0.00	81	652	842	-8.6	good glass, green, mostly clear, one slab with thin skin
TIG-18, A93031	49.00	30.00	0.00	5.00	16.00	0.00	0.00	--	--	--	--	opaque, lt. green yellow color, no glass
TIG-19, A93032	53.00	24.00	0.00	6.00	17.00	0.00	0.00	--	--	--	--	opaque, lt. green color
TIG-20, A93033	32.00	10.00	18.00	10.00	30.00	0.00	0.00	93	630	761	-7.4	yellow green layer of surf. xtals, one slab w/ thin skin
TIG-21, A93034	43.00	27.00	0.00	16.00	14.00	0.00	0.00	--	--	--	--	opaque, lt. green color
TIG-22, A93035	45.00	14.00	0.00	10.00	31.00	0.00	0.00	97	--	--	--	most of bulk xtallized, glass on quenched surface
TIG-23, A93036	37.00	15.00	11.00	14.00	23.00	0.00	0.00	89	646	803	-8.4	greenish tint, thin skin of white surface xtals.
TIG-23, A93039	37.00	15.00	11.00	14.00	23.00	0.00	0.00	90				greenish tint, thin skin of white surface xtals.
TIG-23, A94029	37.00	15.00	11.00	14.00	23.00	0.00	0.00					greenish tint, thin skin of white surface xtals.
TIG-24, A93040	31.45	17.30	40.88	0.00	10.38	0.00	0.00	92	662	779	<-10	good glass, goldish olive color. bubble swirls in slabs
TIG-25, A93041	49.26	9.85	24.63	0.00	16.26	0.00	0.00	79	650	743	-7.6	good glass, brownish, mostly clear. some bubbles, surf. xtals.
TIG-26, A93042	57.31	11.46	12.31	0.00	18.91	0.00	0.00	78	657	817	-7.3	excellent glass, light gold, no surf. xtals, few bubbles
TIG-27, A93043	41.25	8.25	9.26	0.00	41.25	0.00	0.00	109	625	680	-6.5	lt. yellow green, thin film surf. xtals.
TIG-28, A93044	42.32	23.28	20.44	0.00	13.97	0.00	0.00	--	--	--	--	opaque, no glass
TIG-29, A93045	34.61	19.04	11.75	0.00	34.61	0.00	0.00	--	--	--	--	opaque, no glass
TIG-30, A93068	32.00	15.50	12.30	16.60	23.60	0.00	0.00	--	--	--	--	opaque, eige, did not form glass
TIG-31, A94004	32.00	15.50	12.30	16.60	7.80	7.90	7.90	(89)	--	--	--	opaque, white, thin skin of milky glass on quench surf.
TIG-32, A94005	57.00	9.00	0.00	12.00	22.00	0.00	0.00	76	645		-7.0	excellent elms. sit. bluish green tint
TIG-33, A94010	32.00	14.70	0.00	15.80	33.50	0.00	0.00	(91)				opaque, brown, thin layer of glass on quench surf.
TIG-34, A94013	37.00	15.00	11.00	14.00	11.50	11.50	0.00	86	656	790	-8.9	sit. green tint. very thin film of surface xtals.
TIG-35, A94026	37.00	15.00	11.00	14.00	11.50	0.00	11.50	(92)				opaque yellow green. Xtallized interior, glassy quenched surface
TIG-36, A94044	37.00	15.00	11.00	14.00	10.00	0.00	13.00	(92)				opaque white
TIG-37, A94045	51.00	15.00	12.00	5.00	5.00	0.00	12.00	--	--	--	--	opaque white/yellow white, maybe xtalline/phase sep.
TIG-38, A94050	37.00	15.00	11.00	9.00	23.00	5.00			(631)	(820)	-8.9	very dark brown glass

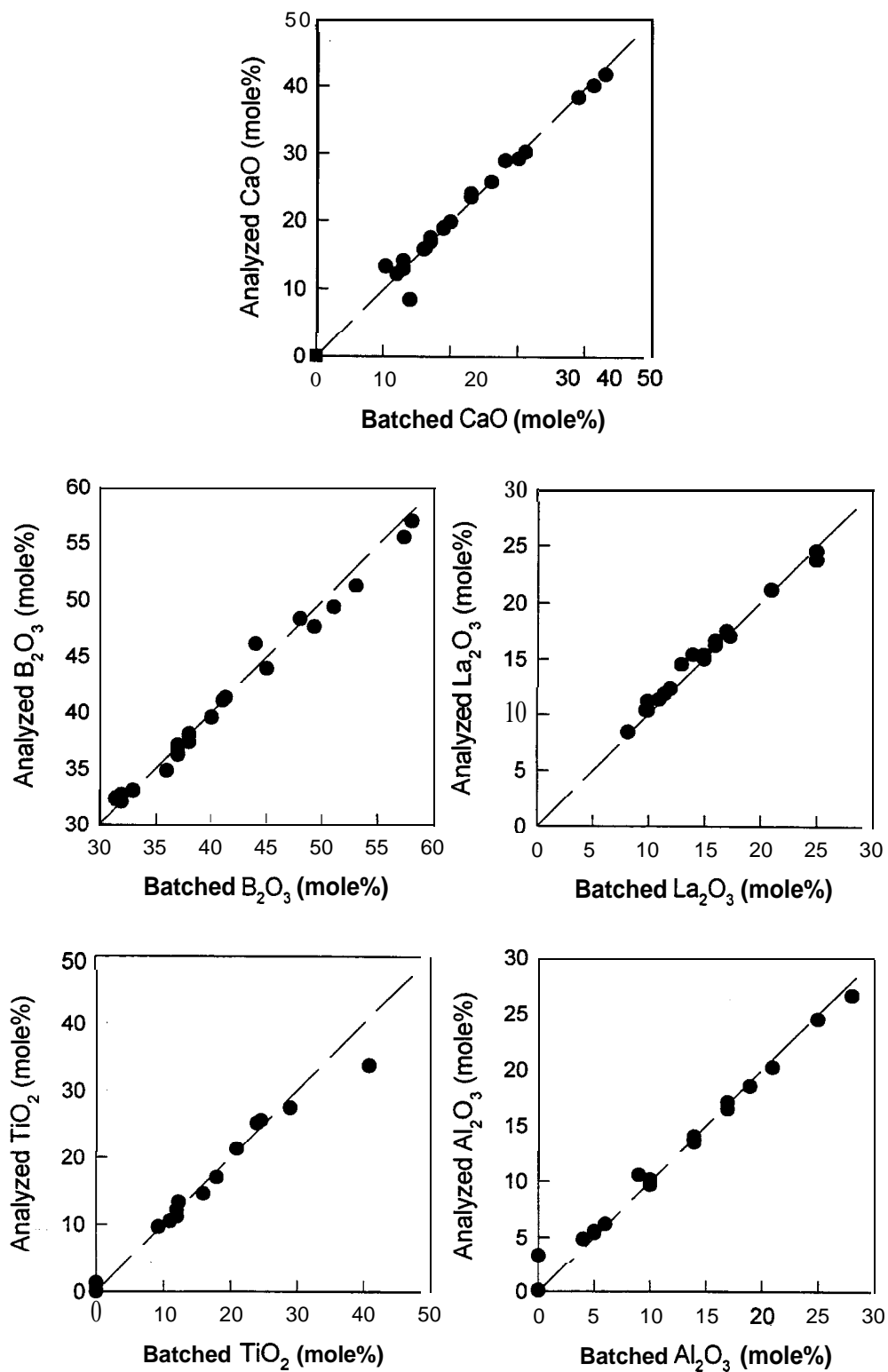


Figure 3.1: Comparisons of the batched and analyzed compositions of the glasses prepared for the experimental design.

These models were used to predict optimum compositions for a set of desired properties. For example, TIG-30 (Table 3.2 below) is the composition with the greatest AT and a CTE between 90 and 100x 10⁻⁷/°C. The predicted B₂O₃-content is the minimum allowed by the model. As a consequence, this composition partially devitrified when quenched. (X-ray diffraction showed that the LaBO₃ was the primary crystalline phase, along with minor amounts of CaTiO₃ and Ca₃Al₂O₆). A second example is TIG-32, a TiO₂-free composition with a maximized greatest AT and a CTE between 70 and 80 x 10⁻⁷/OC; this composition exhibited no devitrification. A comparison of the predicted and actual properties for these two glasses indicates that the mixtures design model can adequately predict properties in the five-component system.

Table 3-2: Sealing glass compositions from the experimental design.

	TIG-30	TIG-32
B ₂ O ₃	32.0	57.0
La ₂ O ₃	15.5	9.0
TiO ₂	12.3	0.0
Al ₂ O ₃	16.6	12.0
CaO	23.6	22.0
CTE (predicted)	90x 10 ⁻⁷ /°C	70x 10 ⁻⁷ /°C
CTE (measured)	90x 10 ⁻⁷ /°C	76X 10 ⁻⁷ /°C
AT (predicted)	159°C	254°C
AT {measured)	154°C	no crystal.
logDR (predicted)	-8.7	-5.7
logDR (measured)	not measured	-7.0

These five-component glasses generally tend towards crystallization during sealing. Nevertheless, we did have some success making simple, hermetic Ti pin seals using some of these compositions (described below). As a result, we filed a Technical Advance titled *Durable Glasses for Titanium Hermetic Seals* (S-80,81 1, SD-5363, Jan. 7, 1994).

III.2 Additional Lanthanoborate Sealing Compositions

During the course of our characterization of the alkaline earth lanthanoborate glasses, we noted that the BaO-glasses in particular were less prone to crystallization than the ‘TIG’ glasses described above, while retaining superior corrosion resistance to the alkaline earth aluminoborates previously developed for Ti seals [Brow and Watkins 1992]. The basic ternary compositions were modified with several additional oxides; compositional ranges are given in Table 3-3 and specific compositions of glasses examined thus far are given in Table 3-4.

Table 3.3: Approximate compositional ranges (in mole%) for new glasses for titanium hermetic seals.

Li ₂ O	Na ₂ O	CaO	BaO	Al ₂ O ₃	La ₂ O ₃	TiO ₂	SiO ₂	B ₂ O ₃
0-8	0-8	0-12	5-30	0-20	5-20	0-15	0-8	40-70

Table 3.4: Compositions (in mole%) of representative glasses for titanium sealing applications

Glass	Li ₂ O	Na ₂ O	CaO	BaO	Al ₂ O ₃	La ₂ O ₃	TiO ₂	SiO ₂	B ₂ O ₃
BLB-8	3.0	3.0	0.0	20.7	5.0	5.0	0.0	0.0	63.3
BLB-9	5.0	0.0	0.0	15.0	0.0	10.0	0.0	5.0	65.0
TIG-23M	5.0	0.0	9.0	9.0	10.0	10.0	11.0	2.0	44.0
BLB-10	5.0	5.0	0.0	20.0	5.0	5.0	5.0	0.0	55.0
BLB-12	5.0	0.0	9.0	9.0	4.0	8.0	11.0	0.0	54.0

Important properties for these new glasses are given in Table 3-5, where they are compared with properties of previously developed titanium sealing glasses. Coefficients of thermal expansion (CTE) are generally reported from dilatometry measurements between 50°C and 500°C. The glass transition temperature (T_g) is taken from the same dilatometry curve. Crystallization temperatures (T_x) are taken from the onset of exothermic peaks by differential thermal analysis (DTA). Dissolution rates (DR) are from weight loss measurements in de-ionized water at 70°C, usually after two weeks. In general, the new glasses have lower T_g s and comparable, or higher, T_x s than the 'TIG' glasses reported in our frost TA [Brow et al. 1994b] and described in 111-1. This wider temperature difference ($T_x - T_g$) makes the new glasses much easier to seal. (Sealing is generally done about 200°C above T_g .) The TIG glasses tend to crystallize during the sealing process before adequate glass flow has occurred. The new glasses have superior resistance to attack by de-ionized water compared to the 'RBAL' glasses reported in reference [Brow and Watkins 1992], but poorer aqueous durability than the 'TIG' glasses. The new glasses have a good range of CTES, and so could be used with a variety of desirable pin materials, including titanium, alloy-52, and molybdenum.

Two alkaline earth lanthanoborate glasses, BLB-8 (Table 3-4) and a ternary CaO-lanthanoborate composition (BLC-6: 20CaO•10La₂O₃•70B₂O₃) were tested for their lithium corrosion resistance using the 150°C Li Contact Ampoule Test (LICAT) [Douglas and Bunker 1987]. Both samples exhibited black corrosion products after 24 hours on test. Alkaline earth aluminoborate glasses, on the other hand, exhibit enhanced resistance to attack by lithium and so have found applications as encapsulating seals for lithium electrolytes in Li batteries [Brow and Watkins 1991]. Both of the lanthanoborate glasses contain relatively higher B₂O₃-contents (>60 mole%) than the typical aluminoborates used in Li-corrosion resistant seals (≤50 mole%). The resulting additional trigonal B-sites, which are believed to be preferentially corroded, might make these particular lanthanoborates susceptible to attack by lithium metal.

Hermetic seals have been made with BLB-8 and titanium bodies with titanium pins (described below) and a second Technical Advance, titled *Improved Glasses for Low Temperature Hermetic Seals to Titanium* [Brow 1995], was filed.

Table 3.5: Selected properties of different borate-based titanium sealing glasses.

Glass	CTE (10 ⁻⁷ /°C)	T _g (°C)	TX (°C)	DR (g/cm ² •min)	reference
BLB-8	94	533	800	3.2x 10 ⁻⁰	present
BLB-9	87	584	739	2.5 X 10 ⁻¹	present
TIG-23M	92	561	832	1.8x 10 ⁻¹	present
BLB-10	103 (450°C)	506	677	6.0 X 10 ⁻¹	present
BLB-12	9 0	562	765	3.9 x 10 ⁻¹	present
SrBAI-1	98	575	805	2X 10 ⁻⁴	Brow and Watkins 1992
BABAL-2	104	542	--	1 x 10 ⁻¹	Brow and Watkins 1992
CABAI-17	91	592	-800	1 x 10 ⁻²	Brow and Watkins 1992
TIG-17	81	652	842	3 x 10 ⁻¹	present
TIG-23	89	646	803	4X 10 ⁻¹	present
TIG-24	92	662	779	<1 x 10 ⁻⁹	present

III-3 Titanium Sealing

Initial titanium sealing experiments were done using ‘TIG’ glasses from the mixtures design experiment described above. In particular, seals were made using TIG-23, the centroid composition from the experimental design. This composition has a thermal expansion coefficient (89 x 10⁻⁷/°C) close to that for titanium (Ti (grade 4) has a CTE from room temperature to 650°C of 93.9 x 10⁻⁷/°C whereas that for Ti-6Al-4V is 95.1 x 10⁻⁷/°C), a reasonably large AT (-150°C) to minimize crystallization during sealing, and an excellent resistance to corrosion by water (weight loss rate in 70°C deionized water, -4 x 10⁻⁹g/cm²-min, comparable to conventional silicate sealing glasses).

Split preforms for a D-cell header (Figure 3-3) were cast from aTIG-23 melt (93-036). Both grade 4 titanium and Ti-6Al-4V pins were used with 304 stainless steel headers (32.5 mm OD, 62.5 mm ID). Weighted graphite fixtures were used to position the glass (1 .37 g plunger with a 5-gram weight). A titanium box, fashioned from 10-roil sheet stock, was used to reduce oxidation of the sealed parts. Seals were made in a batch furnace with an Argon atmosphere using the following thermal cycle:

- . Heat to 775°C at 25 °C/min.;
- Hold at 775°C for 15 minutes;
- Cool to 640°C at 15 °C/min.;
- . Hold at 640°C for 15 minutes;
- . Cool to 600°C at 5°C/min.;
- . Cool to room temperature at 1 0°C/min.

Seals made in this fashion were hermetic to He leak rates <1 x 10⁻⁹ cc-He/sec.

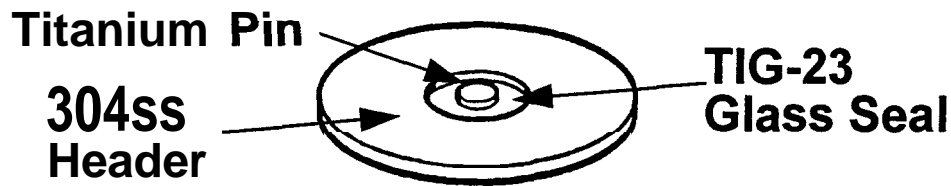


Figure 3-2: D-cell configuration used to fabricate titanium seals.

A second, matched configuration was also examined (Figure 3-3). The seals were made using solid glass preforms of BLB-8 (Table-3.4) machined from melt-cast rods. The bodies, pins, and preforms were again aligned using graphite fixtures and seals were made in a batch furnace at 725°C for 10 minutes. A second set of seals were made in the belt furnace set at 735°C with a nitrogen atmosphere. In both cases, seals could be made without using a top weight to aid glass flow, an advantage over processing 'RBAI' glasses which do not exhibit adequate flow without weights. Seals made with BLB-8 are hermetic to He-leak rates $<1 \times 10^{-9}$ cc-He/min and have survived three thermal shock cycles from -50°C to +150°C.

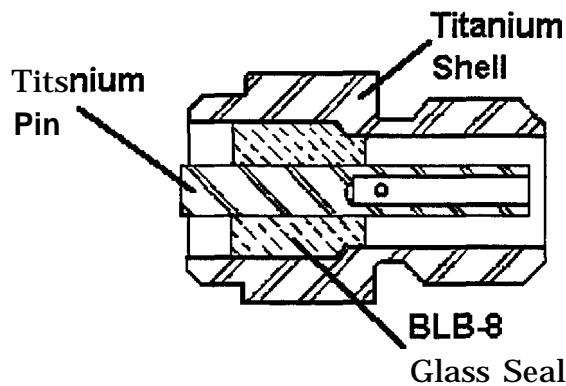


Figure 3-3: Titanium seal made with improved sealing glass.

Finally, several seals were made with titanium shells and pins using BLB-8 glass for a prototype header for a biomedical device company. Again, graphite fixtures were used. Seals were made at 800°C in a batch furnace and in a belt furnace with an Argon atmosphere. The higher processing temperature resulted in some carbon transfer; based on the batch furnace results noted above, this temperature could be reduced for future belt-processed seals. Nevertheless, the seals were hermetic to 10^{-9} cc-He/sec and passed a 500 volt (DC) insulation resistance breakdown test.

IV. Glass/Titanium Interracial Reactions

Titanium is a reactive metal that rapidly reduces silicate glasses during sealing, typically at temperatures over 900°C, to form a silicide interracial reaction product. The poor adherence of the glass to this silicide is believed responsible for the poor mechanical performance of Ti/silicate glass seals [Brow and Watkins 1987]. Borate glasses undergo similar reduction reactions to form an interracial boride [Brow and Watkins 1987, Brow *et al.* 1993]. However,

the extent of these reactions is significantly less and so they do not have a deleterious effect on the mechanical integrity of the seal [Brow and Watkins 1987].

The goal of this part of our research program was to characterize the interracial reactions of silicate and borate glasses with titanium. This work was done primarily at Lehigh University in collaboration with Prof. Himanshu Jain under contracts AO-4 108, AJ-0985, and AF-0924, and resulted in a PhD. dissertation. Analytical electron microscopic, x-ray diffraction, and quantitative x-ray photoelectron spectroscopic techniques were developed to characterize reaction products between model silicate and borate glasses and Ti. What follows is a summary of the Lehigh University research. A detailed discussion of this work can be found in reference [Saha 1996].

R/-I. Ti/Glass Interracial Analyses

Binary sodium silicate ($\text{Na}_2\text{O}\cdot 2\text{SiO}_2$) and sodium borate ($\text{Na}_2\text{O}\cdot 2\text{B}_2\text{O}_3$) glasses were prepared using conventional melt techniques. Contact angles on pure titanium substrates, after two hours at temperature, were determined in a fused silica tube furnace under flowing, gettered ultra-high purity argon and are reported in Table 4-1. Clearly, the borate glass wets titanium better than the silicate glass.

Table 4-1: Equilibrium contact angles for binary glasses on titanium.

	$\text{Na}_2\text{O}\cdot 2\text{SiO}_2$	$\text{Na}_2\text{O}\cdot 2\text{B}_2\text{O}_3$
650°C	nm	34°
900°C	86°	~26°
950°C	nm	14°
1000°C	80°	<14°
1150°C	69°	nm

A variety of samples were prepared to study interracial reactions between these binary glasses and titanium. Among these include diffusion couples heated to 1000°C for 24 hours. Figure 4-1a and 4-1 b shows scanning electron micrographs of a NSi_2/Ti interface and a NB_2/Ti interface, respectively. There is a distinct difference in the reaction morphologies. A planar $\text{Ti}_5\text{Si}_3(\text{O})$ layer, identified by x-ray diffraction, forms on the Ti-side of the silicate glass couple, whereas discontinuous TiB precipitates (also identified by XRD) are observed extending into the Ti side of the borate glass reaction couple. XRD also reveals the presence of Ti_2O at the NB_2/Ti interface; no crystalline oxides were detected at the NSi_2/Ti interface. Diffusion couples prepared between B_2O_3 glass and Ti, as well as more complex aluminoborate glasses and Ti [Brow et al. 1993] possess similar TiB interracial precipitates.

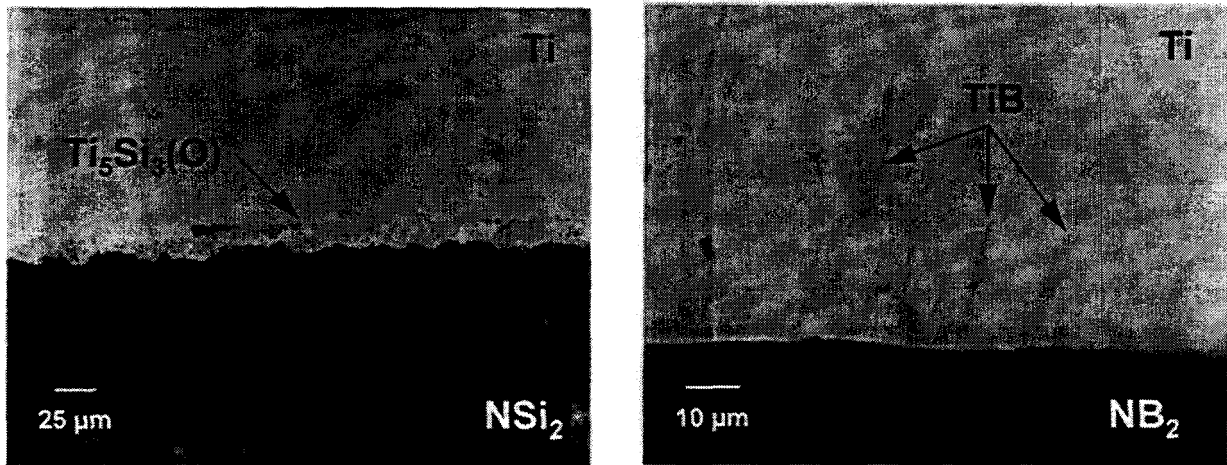


Figure 4-1: Micrographs of titanium/glass reaction interfaces. a) SEM micrograph of the interface of a $\text{Na}_2\text{O}\cdot 2\text{SiO}_2/\text{Ti}$ diffusion couple, and b) SEM micrograph of the interface of a $\text{Na}_2\text{O}\cdot 2\text{B}_2\text{O}_3/\text{Ti}$ diffusion couple. Both samples were held at 1000°C for 24 hours. Note the different scales.

X-ray diffraction was performed on a variety of glass/Ti reaction couples, heated at 700°C or 1000°C , from 2 to 246 hours. An example of the diffraction pattern collected from a Ti/CGW0080, heated at 1000°C for two hours, is shown in Figure 4-2 (CGW0080 is a soda lime silicate glass manufactured by Corning, Inc., and is similar to glasses recommended for Ti/glass seals [Kohl, 1967].) Ti_5Si_3 , along with unreacted Ti, can be identified from this pattern. Crystalline Ti_5Si_3 , Ti_2O , Ti_2O_3 , and TiO_2 are all examples of reaction products detected in Ti/ SiO_2 and Ti/ $\text{Na}_2\text{O}\cdot 2\text{SiO}_2$ diffusion couples. B_2O_3 glass showed no evidence for reaction with Ti, even after 89 hours at 700°C . (By contrast, Ti_5Si_3 could be detected in a SiO_2 glass diffusion couple after 3 hours at 700°C .) Crystalline TiB_2 was identified in a Ti/ $\text{Na}_2\text{O}\cdot 2\text{B}_2\text{O}_3$ diffusion couples after 3 hours at 700°C .

The conditions required to create reaction products of sufficient size to be characterized by analytical scanning electron microscopic and x-ray diffraction techniques are clearly not representative of the much shorter times, and generally lower temperatures, employed to create a glass/Ti seal. X-ray photoelectron spectroscopy has proved useful to characterize the significantly thinner reaction products that form at a seal interface [Brow and Watkins 1987] and it was used in the present study to characterize the initial interracial reactions of simple silicate and borate glasses with titanium.

Titanium films, generally $\sim 30\text{\AA}$ thick, were deposited on glass surfaces fractured *in vacuo* and analyzed, before and after heat treatments, again performed *in vacuo*, at temperatures up to 500°C . Experimental procedures and equipment are described in detail in [Saha 1996].

Figure 4-3a shows the Si2p photoelectron spectrum from a SiO_2 glass after Ti deposition at room temperature. The intense peak centered near 103.6 eV is due to silicon atoms in the glass bonded to oxygens. A lower intensity, asymmetric peak near 97 eV is due to a silicide phase that results from a reduction reaction between the Ti film and the glass substrate. Similar room temperature reactions occur when Ti films are deposited on $\text{Na}_2\text{O}\cdot 2\text{SiO}_2$ glass substrates.

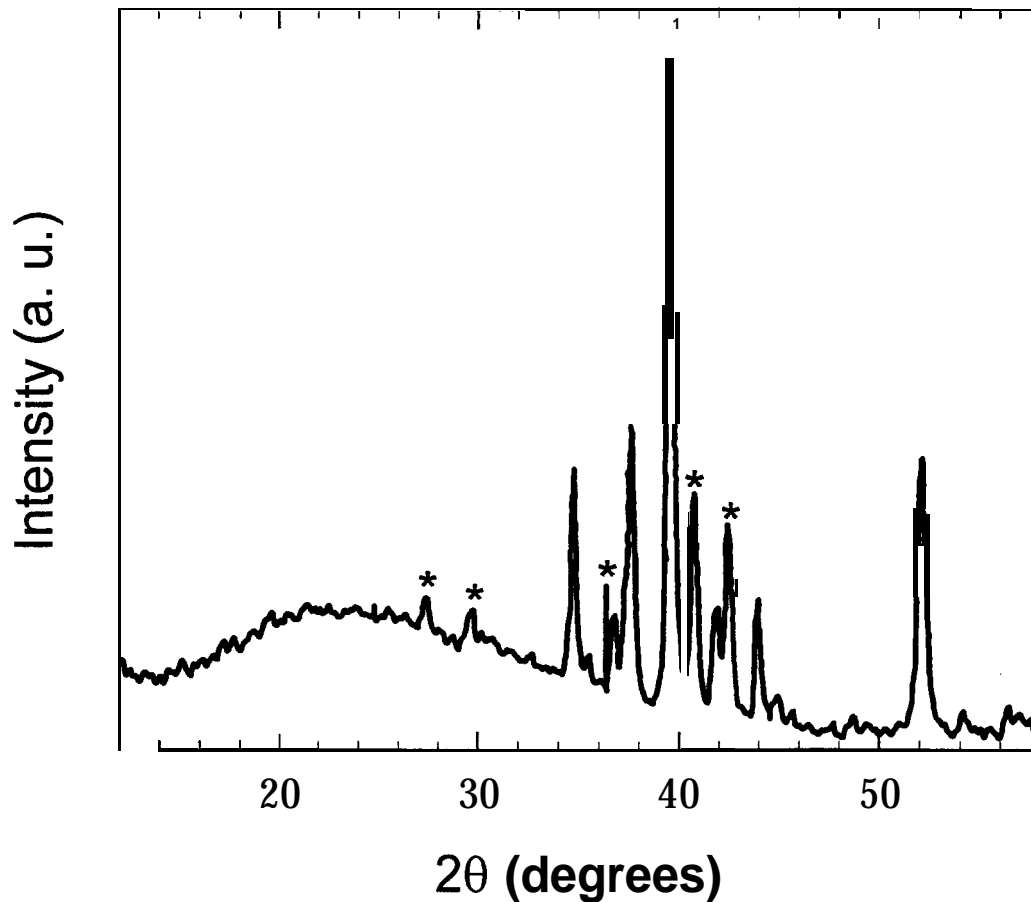


Figure 4-2: X-ray diffraction pattern from a Ti/silicate glass diffusion couple. The Ti/CGW0080 powder diffusion couple was heated at 1000°C for two hours. Asterisks mark peaks due to Ti_5Si_3 , remaining peaks are due to unreacted α -Ti.

Similar room temperature reduction reactions occur when Ti is deposited onto the borate glass substrates. Figure 4-3b shows the B1s photoelectron spectrum from aB_2O_3 glass after Ti deposition at room temperature. The intense peak centered near 193 eV is due to oxidized boron and the lower intensity peak near 186 eV, not present in the spectrum from an ‘as fractured’ glass prior to Ti deposition, is due to a thin boride reaction product.

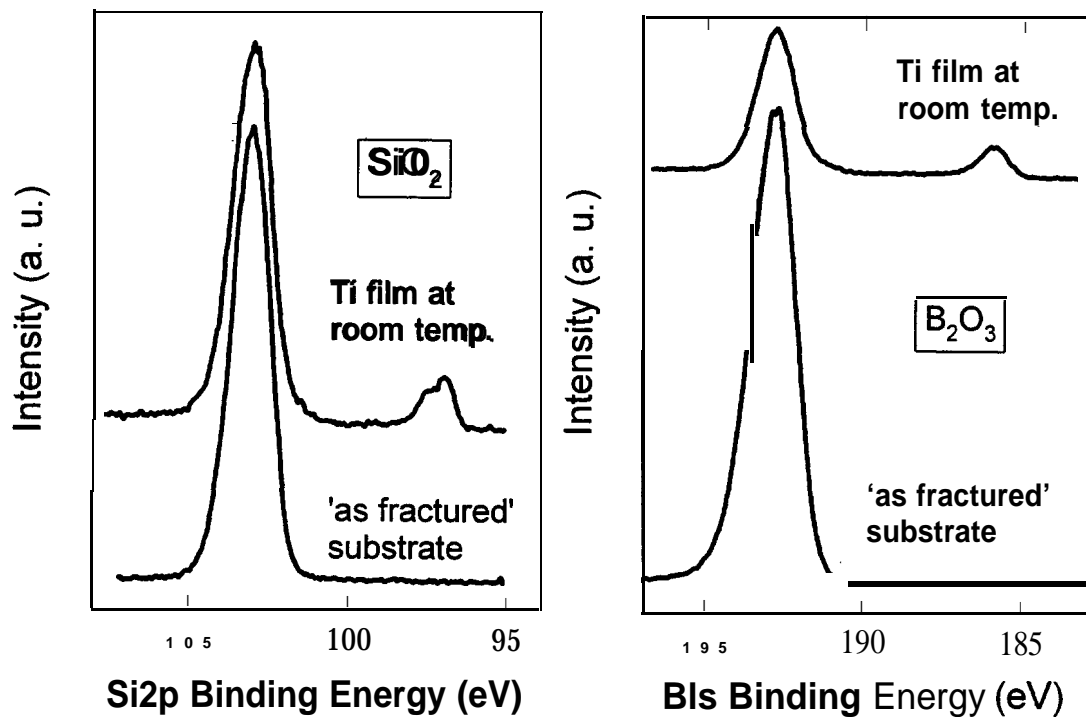


Figure 4.3: Photoelectron spectra from Ti/glass interfaces. a) SiO₂ substrate, and b) B₂O₃ substrate. Both were first fractured in vacuum (bottom two “spectra”) and then were coated with a ~30Å Ti film at room temperature (top two spectra).

IV-2. Ti/ Glass Reaction Summary

The analyses reported by Saha in [Saha 1996] lead to the following observations about glass/Ti bonding. A titanium silicide phase with a large Ti stoichiometry forms at the interface between Ti and every silicate glass examined. The Ti/Si ratio in this silicide decreases as the reaction progresses until Ti₅Si₃(O) forms. Further reactions, particularly when alkali and alkaline earth oxides are present in the glass, can lead to the decomposition of the silicide to form Ti-oxides. The diffusion of Ti through the silicide layer and the release of oxygen during the reduction reactions is thought to control the relative reaction layer thickness and stoichiometry. Interestingly, the Ti-oxides do not format the interface between the glass and metal, as is typical for a well-bonded glass-metal seal [Pask 1987]. In all cases, the silicide is adjacent to the residual glass and this is the interface that separates when a Ti/silicate glass seal fails [Brow and Watkins 1987].

Similar reduction reactions occur at the Ti/borate glass interfaces. As shown above, a boride reaction phase can be detected by XPS even at room temperature. Borate glasses in general, however, are less reactive than silicates and so it is likely that the boride reaction product acts as a diffusion barrier to inhibit further reduction. In addition, the dendritic nature of the Ti-boride reaction products offers a degree of mechanical bonding that is not contributed by

the planar Ti-silicide reaction product (compare Figures 4-1a and 4-1b), thus leading to improved adhesion by the borate glasses. The dendritic morphology is thought to result from the relatively greater diffusivity of B in titanium, compared to Si, and the reaction of the initial TiB_2 layer with Ti to form TiB dendrites. Ti_5Si_3 on the other hand is stable in the presence of Ti and so does not participate in such secondary reactions. Finally, the lower temperatures required for sealing borate glasses will likely result in less oxygen dissolution into the Ti substrate, avoiding the formation of a mechanically weak Ti-oxide layer, as well as reducing the relative thickness of the boride interface, compared to the silicide formed at a necessarily higher silicate glass sealing temperature.

V. Summary and Conclusions

1. Glass formation in several **lanthanoborate** systems has been identified. Spectroscopic studies suggest that glass networks are based on **metaborate** anions, including modified anions that incorporate aluminum or titanium polyhedra. In general, these glasses have the requisite thermal and chemical properties for making seals to titanium alloys, including thermal expansion coefficients in the range $70-100 \times 10^{-7}/OC$ and glass transition temperatures low enough to seal below the allotropic phase transition temperature for Ti. More importantly, these glasses have significantly better resistance to attack by aqueous environments than the alkaline earth **aluminoborate** glasses presently used in some T-sealing applications.
2. Glass formation in Fe- and **Ti-modified** calcium phosphate glasses has been identified. These glasses have remarkably good aqueous durabilities, better than most phosphate glasses. Spectroscopic studies indicate that phosphate chains are cross linked by Fe- or **Ti-polyhedra** to form three dimensional Fe- or **Ti-phosphate** networks.
3. Glass properties in the $CaO-Al_2O_3-TiO_2-La_2O_3-B_2O_3$ system were modeled using a mixtures experimental design and several specific compositions were identified for potential sealing applications. For example, titanium pins were hermetically sealed in stainless steel headers at $775^\circ C$ using solid preforms of TIG-23. The tendency for this glass to crystallize, however, precluded its use with pressed powder preforms unless sealed at temperatures great enough ($1000^\circ C$) to remelt the crystals. Nevertheless, the outstanding aqueous **durabilities** of the 'TIG' glasses make them attractive for some specialty sealing applications.
4. Barium **lanthanoborate** glasses, while possessing relatively poorer aqueous **durabilities** than the 'TIG' glasses, are less prone to crystallization during sealing and robust hermetic seals between titanium pins and headers were made at temperatures as low as $725^\circ C$.
5. The nature of the interracial reaction product seems to most affect the adherence of a glass to titanium. Relatively thick, planar **Ti-silicides** are associated with the debonding of silicate glasses, whereas thin, dendritic **Ti-borides** are present with well-adhered borate glasses.

References

- P. B. Adams, 1990, LaBTi Glasses with Very High Alkali Durability, paper 94-G-90, 92nd Annual Meeting of the American Ceram Society, Dallas, TX, April 22-26.
- C. A. Angell, D. J. List, and J. Kieffer, 1989, Glassforming Liquid Oxides at the Fragile Limit of the Viscosity-Temperature Relationship, *Proc. XV Int. Cong. on Glass, Leningrad*, , p. 204-209.
1. D. Bloom and K. L. Ley, 1995, "Compliant Sealants for Solid Oxide Fuel Cells and Other Ceramics," US Patent 5,453,331, September 26.
- R. K. Brow and R. D. Watkins, 1987, Reactions and Bonding Between Glasses and Titanium, in *Technology of Glass, Ceramic, or Glass-Ceramic to Metal Sealing*, ed. W. E. Moddeman, et al., pp. 25-30, Winter Annual Meeting, Amer. Soc. Mech. Eng., Boston, MA, Dec. 13-18.
- R. K. Brow and R. D. Watkins, 1991, High Expansion Li Corrosion Resistant Sealing Glasses, US Patent 5,104,738, April 14.
- R. K. Brow and R. D. Watkins, 1992, Sealing Glasses for Titanium and Titanium Alloys, US Patent 5,021,307, June 4.
- R. K. Brow, S. K. Saha, and J. I. Goldstein, 1993, Interfacial Reactions Between Titanium and Borate Glass, *Joining and Adhesion of Advanced Inorganic Materials, Proceedings of the Materials Research Society*, Vol. 314, pp. 77-81.
- R. K. Brow, C. M. Arens, X. Yu, and D. E. Day, 1994, An XPS Study of Fe-Phosphate Glasses, *Phys. Chem. Glasses*, vol. 35[3], pp. 132-36.
- R. K. Brow, H. L. McCollister, C. C. Phifer, and D. E. Day, 1994b, Durable Glasses for Titanium Hermetic Seals, *SNL Technical Advance (S-80,811, SD-5363)*, Disclosure Made Jan. 13, 1994.
- R. K. Brow, 1995, Improved Glasses for Low Temperature Hermetic Seals to Titanium, *SNL Technical Advance (S-83,671, SD-5660)*, disclosure made April 18, 1995.
- R. K. Brow, D. R. Tallant, and G. L. Turner, 1996a, Spectroscopic Studies of the Structures of Alkaline Earth Lanthanoborate Glasses, (to be published in *J. Amer. Ceram. Soc.*)
- R. K. Brow, D. R. Tallant, W. L. Warren, A. L. McIntyre, and D. E. Day, 1996b, Spectroscopic Studies of the Structure of Titanophosphate and Calcium Titanophosphate Glasses, submitted to *Phys. Chem. Glasses*.
- B. C. Bunker, R. J. Kirkpatrick, R. K. Brow, G. L. Turner, and C. Nelson, 1991, Local Structure of Alkaline-Earth Boroaluminate Crystals and Glasses: II, ^{11}B and ^{27}Al MAS NMR

- Spectroscopy of Alkaline-Earth Boroaluminate Glasses, *J. Amer. Ceram. Soc.*, vol. 74[6] 1430-38.
- T. Cardinal, E. Fargin, Y. Le Luyer, G. Le Flem, L. Canioni, P. Segonds, L. Sarger, F. Adarnietz, and A. Ducasse, 1995, Contribution of XAFS analysis to the study of the correlation between optical nonlinearity and the geometry of titanium sites in glass, *Nucl. Meth. Phys Res.* vol B97, 169-71.
- I. N. Chakraborty, J. E. Shelby, R. A. Condrate, 1984, Properties and Structure of Lanthanum Borate Glasses, *J. Amer. Ceram. Soc.*, vol. 67, pp. 782-85.
- I. N. Chakraborty, D. E. Day, J. C. Lapp, and J. E. Shelby, 1985, Structure-Property Relation in Lanthanide Borate Glasses, *J. Amer. Ceram. Soc.*, vol. 68, pp. 368-71.
- I. N. Chakraborty and D. E. Day, 1985, Effect of R^{3+} Ions on the Structure and Properties of Lanthanum Borate Glasses, *J. Amer. Ceram. Soc.* vol. 68[12] pp. 641-45.
- G. D. Chryssikos, J. A. Kapoutsis, E. I. Karnitsos, A. P. Patsis, and A. J. Pappin, 1994, Lithium-sodium metaborate glasses: structural aspects and vitrification chemistry, *J. Non Cryst. Solids*, vol. 16792-105.
- D. E. Day, 1991, Titanium Sealing Glass for Biomedical Applications, Final Report/Faculty Sabbatical Leave, June 28.
- D. E. Day and A. L. McIntyre, 1994, Study of Phosphate Glasses (Calcium Iron Phosphates), *Final Technical Report, AF-0923*, Feb. 2.
- D. E. Day, Z. Wu, and A. L. McIntyre, 1994, Biocompatible Phosphate Glasses and Glass Ceramics, *Final Technical Report, AJ-0984*, Nov. 30.
- R. H. Doremus, 1992, Review: Bioceramics, *J. Mater. Sci.*, vol. 27, pp. 285-97.
- S. D. Douglas and B. C. Bunker, 1987, Study of Separator Materials Using the LiCAT (Lithium Contact Ampule Test) Method, *Sandia Report SAND86-1350*, April 1987..
- J. A. Duffy and M. D. Ingram, 1976, An Interpretation of Glass Chemistry in Terms of the Optical Basicity Concept, *J. Non-Cryst. Solids*, vol. 21 pp. 373-410.
- I. Fanderlik, 1983, *Optical Properties of Glass*, p. 96 Elsevier, Amsterdam.
- Z. Feipeng, A. P. Tomsia, and J. A. PaSk, 1980, Wetting and Reactions in Glass/Titanium Systems, in *Proc. 33rd Pacific Coast Meeting Amer. Ceram. Soc.*, held in San Francisco, CA, pp. 76-78.
- R. Fröhlich, 1984, Crystal Structure of the low-temperature form of BaB_2O_4 , *Z. Kristallogr.* vol 168 pp. 109-112.

- K. Fukumi, J. Fukunaga, J. Yoshida, and M. Ihara, 1984, Raman Spectroscopic Study of CaO-Al₂O₃-B₂O₃ Glasses, *Yogyo Kyokai-Shi* vol. 92, pp. 680-685.
- T. Hayashi and H. Saito, 1979, Structure and electrical properties of TiO₂-Ti₂O₃-P₂O₅ glasses, *Phys. Chem. Glasses*, vol. 20[5], 108-114.
- K. Hayashi, N. Matsuguchi, K. Uenoyama, T. Kanemaru, and Y. Sugioka, 1989, *J. Biomed. Mater.* vol. 23, 1247-59.
- L. L. Hench, 1991, Bioceramics: From Concept to Clinic, *J. Amer. Ceram. Soc.*, vol. 74[7], pp. 1487-1510.
- J. T. Hoggins, J. S. Swinnea, and H. Steinfink, 1983, Crystalline Fe₂P₂O₇, *J. Solid St. Chem.*, vol. 47, pp. 278-83.
- T. S. Izumitani, 1986, *Optical Glass*, p. 19, American Institute of Physics Translation Series, New York.
- E. M. Levin, C. R. Robbins, and J. L. Waring, 1961, Immiscibility and the System Lanthanum Oxide-Boric Oxide, *J. Amer. Ceram. Soc.*, vol. 44, pp. 87-91.
- E. I. Karnitsos, M. A. Karakassides, and G. D. Chryssikos, 1987, Vibrational Spectra of Magnesium-Sodium-Borate Glasses. 2. Raman and Mid-Infrared Investigation of the Network Structure, *J. Phys. Chem.*, vol. 91 [5] pp. 1073-1079.
- A. Kishioka, 1978, Glass Formation in the Li₂O-TiO₂-P₂O₅, MgO-TiO₂-P₂O₅, and CaO-TiO₂-P₂O₅ Systems, *Bull. Chem. Soc. Japan*, vol. 51 [9] pp. 2559-2561.
- W. H. Kohl, 1967, *Handbook of Materials and Techniques for Vacuum Devices*, Reinhold Publishing Corp., New York.
- W. L. Konijnendijk and J. M. Stevels, 1975, The Structure of Borate Glasses Studied by Raman Scattering, *J. Non-Crystal. Solids*, vol 18, pp. 307-331.
- N. J. Kreidl, 1983, Inorganic Glass-Forming Systems, in *Glass Science and Technology, Vol. 1*, ed. D. R. Uhlmann and N. J. Kreidl, Academic Press, New York.
- N. J. Kreidl, 1989, Variability of optical properties and structure of glass, *Glastech. Ber.*, vol. 62[6] pp. 213-218.
- E. Mal'shikov and I. A. Bondar', 1989, Phase Formation in the TiO₂-P₂O₅ System, *Izv. Akad. Nauk SSSR, Neorg. Mater. (Engl. Trans.)*, vol. 25[6], pp. 829-832.
- M. Marezio, H. A. Plettinger, and W. H. Zachariasen, 1963, Refinement of the Calcium Metaborate Structure, *Acts Cryst.* vol. 16, pp. 390-392.
- P. McMillan and B. Piriou, 1983, Raman Spectroscopy of Calcium Aluminate Glasses and Crystals, *J. Non-Cryst. Solids* vol. 55, pp. 221-242.

- P. B. Moore and T. Araki, 1972, Johachidolite, $\text{CaAl}[\text{B}_3\text{O}_7]$, a Borate with Very Dense Atomic Structure, *Nature (London)*, *Phys. Sci.* vol. 240, pp. 63-65.
- S. V. Nemilov and L. K. Shmatok, 1967, Study of the Viscosity and Structure of Glasses of the System $\text{ZnO-La}_2\text{O}_3\text{-B}_2\text{O}_3$, *Izv. Akad. Nauk SSSR, Neorg. Mater. (Engl. Trans.)*, vol. 4[12], pp. 1884-88.
- J. A. Pask, From Technology to the Science of Glass/Metal and Ceramic/Metal Sealing, 1987, *Cer. Bull.*, vol. 66, pp. 1587-92.
- A. Passerone, G. Valbusa, and E. Biagini, 1977, The Titanium-Molten Glass System: Interactions and Wetting, *J. Mater. Sci.*, 12[12] pp. 2465-74
- G. F. Piepel, 1992, MIXSOFT-- Mixture Experiment Software, Version 2.0, 649 Cherrywood Loop, Richland, WA 99352.
- C. C. Phifer, F. D. Hardcastle, and R. J. Kirkpatrick, 1992, Structural Studies of Rare-Earth Titanoborate Glasses, paper 52-G-92, 94th Annual Meeting of the American Ceramic Society, Minneapolis, MN, 12-16.
- N. V. Romanova and S. V. Nemilov, 1970, Viscosities of Glasses of the Systems $\text{BaO-B}_2\text{O}_3\text{-La}_2\text{O}_3$ and $\text{CdO-B}_2\text{O}_3\text{-La}_2\text{O}_3$ in the Softening Region, *Izv. Akad. Nauk SSSR, Neorg. Mater. (Engl. Trans)* vol. 6[7], pp. 1160-1164.
- S. K. Saha, 1996, Reactions Between Titanium and Silicate/Borate Glasses and Their Role in Interface Adhesion. PhD thesis, Lehigh University.
- K. Searstone and J. O. Isard, 1965, The Chemical Durability of $\text{CaO-B}_2\text{O}_3\text{-Al}_2\text{O}_3$ and $\text{CaO-B}_2\text{O}_3\text{-Al}_2\text{O}_3\text{-SiO}_2$ Glasses, *Glass Technol.* vol. 6[6], pp. 184-189.
- R. D. Snee, 1975, Experimental Designs for Quadratic Models in Constrained Mixture. Spaces, *Technometrics*, vol. 17[2], pp. 149-59.
- J. St. Ysker and W. Hoffman, 1970, "Die Kristallstruktur des $\text{La}(\text{B}_3\text{O}_6)$ " *Naturwiss.*, vol. 57, pp. 129-130.
- G. Turner, K. A. Smith, R. J. Kirkpatrick, and E. Oldfield, 1986, Boron-11 Nuclear Magnetic Resonance Spectroscopic Study of Borate and Borosilicate Minerals and a Borosilicate Glass, *J. Magnet. Reson.* vol. 67, pp. 544-550
- R. D. Watkins, B. C. Bunker, S. C. Douglas, R. K. Brow, and E. E. Hellstrom, 1987, Corrosion Resistant Glasses for Use in Lithium Ambient-Temperature Batteries, *Proceedings of the 22nd Intersociety Energy Conversion Engineering Conference*, pp. 1113-1118, Amer. Inst. Aeronaut. Astronaut., Philadelphia, PA, Aug. 10-14.

J. K. West, A. E. Clark, M. B. Hall, and G. E. Turner, 1990, *In Vivo* Bone-Bonding Study of Bioglass[®]-Coated Titanium Alloy, in *Handbook of Bioactive Ceramics, Vol. I*, edited by T. Yamamuro, et al. (CRC Press, Boca Raton, FL,) pp. 161-66.

Appendix A

Publications

1. R. K. Brow, C. M. Arens, X. Yu, and D. E. Day, "An XPS Study of Fe-Phosphate Glasses," *Phys.Chem. Glasses*, 35[3] 132-36 (1994) {SAND92-0583J}.
2. R. K. Brow, S. K. Saha, and J. I. Goldstein, "Interracial Reactions Between Titanium and Borate Glass," *Joining and Adhesion of Advanced Inorganic Materials, Proceedings of the Materials Research Society*, Vol. 314, pp. 77-81 (1993) {SAND92-2779C}
3. X. Yu, D. E. Day, G. L. Long, and R. K. Brow, "Structure and Properties of Sodium-Iron-Phosphate Glasses," submitted to *J.Non-Cryst. Solids* (1994) {SAND93-1751J}.
4. R. K. Brow, D. R. Tallant, and G. L. Turner, "Raman and ^{11}B NMR Spectroscopic Studies of Alkaline Earth Lanthanoborate Glasses," accepted by *J.Amer. Ceram. Soc.* {SAND95-0967J}.
5. S. K. Saha, H. Jain. A. C. Miller, and R. K. Brow, "XPS Characterization of *In situ* Prepared Ti/Glass Interfaces," *Surf. Interface Analyses*, 24113-118 (1996). {SAND95-2361J}.
6. S. K. Saha, H. Jain. A. C. Miller, and R. K. Brow, "Study of reactions between titanium and silicate glasses by x-ray photoelectron spectroscopy," submitted to *Journal of Vacuum Science and Tech A* {SAND95-2368J}
7. R. K. Brow, D. R. Tallant, and G. L. Turner, "Polyhedral Arrangements in Lanthanum Aluminoborate Glasses," submitted to the *Journal of the American Ceramic Society*.
8. R. K. Brow, D. R. Tallant, W. L. Warren, A. McIntyre and D. E. Day, "Spectroscopic Studies of the Structure of Titanophosphate and Calcium Titanophosphate Glasses," submitted to *Physics and Chemistry of Glass*.
9. S. K. Saha, H. Jain, A. C. Miller, and R. K. Brow "Reaction Between Titanium and B_2O_3 Melt/Glass," submitted to *Physics and Chemistry of Glass*.

Presentations

1. C. M. Arens, R. K. Brow, X. Yu and D. E. Day, "An XPS Study of Bonding in Iron Phosphate Glass", 95th Annual Meeting of the American Ceramic Society, Cincinnati, OH, April 18-22, 1993 {SAND92-2775A}
2. S. K. Saha, J. I. Goldstein, and R. K. Brow, "Analysis and Modeling of Titanium-Borate Glass Reactions," Materials Research Society Spring 1993 Meeting, San Francisco, CA, April 12-16, 1993. {SAND92-2779A}
3. R. K. Brow, D. R. Tallant, and D. N. Bencoe, "Raman and Fluorescence Spectroscopic Studies of Alkaline Earth Lanthanoborate Glasses," 96th Annual Meeting of the Amer.

Ceram. Soc., Indianapolis, IN April 24-28, 1994. {SAND93-4056A}.

4. A. L. McIntyre, R. K. Brow, and D. R. Tallant "Properties and Structure of Calcium Titanophosphate Glasses," 96th Annual Meeting of the Amer. Ceram. Soc., Indianapolis, IN April 24-28, 1994. {SAND93-4016A}.
5. R. K. Brow, "Glass Research at Sandia National Labs," (INVITED), Alfred University, Alfred, NY, Sept. 29, 1995.
6. R. K. Brow and D. R. Tallant, "Oxygen Bonding and Polyhedral Arrangements in Transition Metal Oxide/Phosphate Glasses," 97th Annual Meeting of the Amer. Ceram. Soc., Cincinnati, OH April 30-May 4, 1995. {SAND94-3034A}.
7. S. K. Saha, H. Jain, and R. K. Brow, "Adherence Aspects in Titanium-Borate and Titanium-Silicate Glass," 97th Annual Meeting of the Amer. Ceram. Soc., Cincinnati, OH April 30-May 4, 1995. {SAND94-3037A}.
8. S. K. Saha, H. Jain, A. C. Miller, J. I. Goldstein, and R. K. Brow, "XPS Investigation of Reaction Between Titanium Thin Films and Silicate Glass Substrates," 97th Annual Meeting of the Amer. Ceram. Soc., Cincinnati, OH April 30-May 4, 1995. {SAND94-3038A}.
9. S. K. Saha, H. Jain, A. C. Miller, J. I. Goldstein, and R. K. Brow, "Characterization of titanium and glass interracial reactions using a novel XPS procedure," 17th Annual Symposium on Applied Surface Analysis, Penn State University, University Park, PA, June 6-9, 1995 {SAND95-0792A}.
10. R. K. Brow, L. Kovacic, and R. S. Chambers, "Glass Sealing," Russian/US Workshop on Fuel Cell Technology, Albuquerque, NM, Sept. 27, 1995

Patents/Technical Advances

1. R. K. Brow, H. L. McCollister, C. C. Phifer, and D. E. Day, "Durable Glasses for Titanium Hermetic Seals," S-80,811, SD-5363, (Disclosure Made Jan. 13, 1994; patent filed Sept. 13, 1996).
2. R. K. Brow, H. L. McCollister, C. C. Phifer, and D. E. Day, "Improved Glasses for Low Temperature Hermetic Seals to Titanium," S-83,671, SD-5660 (Disclosure Made April 18, 1995; patent filed Sept. 13, 1996).

Thesis

1. S. K. Saha, "Reactions between Titanium and Silicate/Borate Glasses and Their Role in Interface Adhesion," submitted for a PhD in Materials Science and Engineering, Lehigh University, April 1996.

Distribution

Unclassified, Unlimited Release

1	MS 9018	Central Technical Files, 8523-2
5	0899	Technical Library, 4414
2	0619	Review & Approval Desk, 12630 For DOE/OSTI
1	MS 0188	LDRD Office, 4523
20	MS 1349	R. K. Brow, 1833
1	1411	D. R. Tallant, 1823
1	0829	S. V. Crowder, 12323
1	0367	B. K. Damkroger, 1833
1	1411	J. Phillips, 1823
1	0829	K. V. Diegert, 12323
1	1349	D. N. Bencoe, 1833
1	0959	F. P. Gerstle, 1492
1	0959	T.V. Montoya, 1492
1	0959	S. D. Rospopo, 1492-3
1	0959	R. G. Stone, 1492-3
1	0419	C. C. Phifer, 5412
1	0871	H. L. McCollister, 14466